

## Mechanics of biological networks: from the cell cytoskeleton to connective tissue

Cite this: *Soft Matter*, 2014, **10**, 1864

Robyn H. Pritchard,<sup>a</sup> Yan Yan Shery Huang<sup>b</sup> and Eugene M. Terentjev<sup>\*a</sup>

From the cell cytoskeleton to connective tissues, fibrous networks are ubiquitous in metazoan life as the key promoters of mechanical strength, support and integrity. In recent decades, the application of physics to biological systems has made substantial strides in elucidating the striking mechanical phenomena observed in such networks, explaining strain stiffening, power law rheology and cytoskeletal fluidisation – all key to the biological function of individual cells and tissues. In this review we focus on the current progress in the field, with a primer into the basic physics of individual filaments and the networks they form. This is followed by a discussion of biological networks in the context of a broad spread of recent *in vitro* and *in vivo* experiments.

Received 2nd November 2013  
Accepted 7th January 2014

DOI: 10.1039/c3sm52769g  
[www.rsc.org/softmatter](http://www.rsc.org/softmatter)

### 1 Introduction

Fibrous networks have long been life's structure of choice in building dynamic structures of tunable strength, elasticity, and nonlinear response.<sup>1–4</sup> From the microscopic scale of the cell cytoskeleton to the macroscale of fibrous tissues, biology has come to the solution of utilising stiff and semiflexible filaments, allowing for dynamic remodelling,<sup>5,6</sup> controlled structural failure,<sup>7,8</sup> and enzyme or cell accessible structural elements.<sup>9,10</sup> In this review, we examine the current research on how fibrous networks achieve the rich mechanical behaviour seen in biology. We examine how the mechanics at a single filament level (such as an actin filament or a collagen fibril) can be translated across to the cytoskeleton or/and the tissue levels. Particular interest is paid to the strain stiffening response, stiffening tunability, reversible softening, and recoverable network fluidisation. This behaviour reflects the ability of cells and tissues to dynamically adapt to environmental changes. At the same time, signalling networks triggered by mechanical forces have long been known to have a profound impact on the cell fate, where pre-stress is necessary for cell stability,<sup>11</sup> geometry can determine cellular viability,<sup>12</sup> and substrate stiffness can direct stem cell differentiation.<sup>13</sup> Moreover, the mechanical signatures of cells and tissues can act as hallmarks for their health and disease, seeing significance in clinical applications.

To build up towards an understanding of the mechanics of biological networks at the tissue level, this article will begin with a discussion of single filaments in Section 2. Filaments of no molecular details are used as generic models to establish

broad categories of mechanical behaviour. In particular, we focus on semiflexible filaments, as characterised by their comparable persistence length and contour length, because of their particular relevance to many biological filaments. The equilibrium response of semiflexible filaments to stretching and buckling in compression is discussed, as well as their frequency-dependent response. Section 3 then portrays the behaviour of ideal networks made of these simplified filaments. We show how filamentous networks can gain stability through filament bending and pre-stress, and examine how the interaction between filaments ultimately affects the frequency-dependent dynamic response. Theoretical models are introduced to explain some interesting network behaviour, including power-law response and fluidisation. Building on the knowledge of theoretical networks, the mechanics of the cellular cytoskeleton is then discussed in Section 4. We illustrate how the interaction between cytoskeletal filaments of actin, microtubules and intermediate filaments can give rise to a variety of mechanical properties specifically relevant to living cells. Experimental investigations on *in vivo* and reconstructed cytoskeletal networks are examined; for example, we review how lamellipodium can gain remarkable stiffness, and also reversible strain stiffening and softening. By correlating a typical cytoskeletal network structure with the theoretical models outlined in Section 3, one can also explain the different dynamics of the response, as well as the active tuning of the modulus. Moving further into the cell mechanics in Section 5, we first summarise the methods of measuring cell rheology using passive and active approaches. Widely observed experimental effects, such as the cell fluidisation, are explained with the help of popular cell mechanics models, such as the 'glassy worm-like chain' model, the soft glassy rheology model and the tensegrity model. Finally, in Section 6, we discuss hierarchically structured connective tissues. This involves an overview of the mechanical

<sup>a</sup>Cavendish Laboratory, University of Cambridge, Cambridge, CB3 0HE, UK. E-mail: emt1000@cam.ac.uk

<sup>b</sup>Department of Engineering, University of Cambridge, CB2 1PZ, UK

properties of the extracellular matrix containing collagen, elastin and fibrin fibrils with remarkable compound mechanical properties. We then look at how the arrangement and combination of these fibrils result in a spectrum of strain stiffening responses tailored to the mechanical needs of the particular tissue, with illustrative examples of tendon and arterial connective tissue. We follow this with a discussion of a theoretical model of the connective tissue elasticity.

## 2 Single filaments

Many biological filaments, such as actin, intermediate filaments, microtubules and fibrin, are classed as semi-flexible. Their defining feature is a large persistence length,  $L_p$ , which is comparable to the typical filament contour length,  $L_c$ . The persistence length is intuitively characterised by the length at which thermal energy,  $k_B T$ , is sufficient to bend the filament and reverse its direction; however, it is more formally defined as the separation between two tangent vectors at which their correlation falls by a factor of  $1/e$ . Fig. 1 shows three filaments of increasing  $L_p/L_c$  ratio.

When  $L_p/L_c \ll 1$ , thermal energy is sufficient to bend the filament dramatically, leading to a coil formation of self-avoiding random walk, where the entropic elasticity dominates. When  $L_p/L_c \gg 1$ , thermal energy cannot significantly bend the filament, leaving it in a rigid rod conformation where elasticity is dominated by the potential energy arising from the stretching of molecular bonds. Between these two extremes is the broad regime of semiflexibility, where the end to end distance  $R$  is such that both ratios  $R/L_c$  and  $R/L_p$  could be of order unity, *i.e.* the chain is relatively straight but the thermal energy is enough to cause transverse undulations (see Fig. 1).

As opposed to individual flexible and rigid filaments, semi-flexible filaments exhibit a nonlinear strain response. Strictly,

both the flexible entropic and the rigid elastic filament also have nonlinear elastic regimes: respectively, when the random coil is stretched such that  $R/L_c \sim 1$  and when molecular bonds are stretched so much that the anharmonicity of the potential energy becomes relevant. However, both such regimes are ‘unnatural’ – *i.e.* taking the original object outside of its nominal definition range, in contrast to semiflexible filaments where the nonlinear elasticity is a natural consequence of the comparable characteristic length scales. The response is well understood in terms of the worm like chain (WLC) model, which defines a filament as an inextensible curve with an energy penalty for bending. Fig. 1 shows such a curve, where  $\mathbf{r}(s, t)$  defines the path the curve takes in space and time, and is parameterised by  $s$ , the arc length along the curve. The end to end extension can be defined by a dimensionless quantity,  $x = R/L_c$ .

The standard approach to find the elastic response of a semiflexible filament is to use the WLC model to construct the filaments’ partition function. With this one may calculate the free energy:  $F(x) = -k_B T \ln P(x)$ , where  $P(x)$  is the partition function, *i.e.* the statistical weight of the filament fluctuating at fixed  $x$ , and is equivalent to the probability that ends of the filament are separated by  $R = xL_c$ . The partition function is given by the relation:  $P(x) \propto \int \mathcal{D}\mathbf{r}(s) \exp(-H[\mathbf{r}(s)]/k_B T)$ , where  $H[\mathbf{r}]$  is the Hamiltonian of the WLC, and in the simplest approximation given by

$$H[\mathbf{r}(s)] = \frac{1}{2} \int_0^{L_c} ds A \left( \frac{d^2 \mathbf{r}}{ds^2} \right)^2, \quad (1)$$

where  $\|d^2\mathbf{r}/ds^2\|$  is the local curvature and  $A$  is the modulus associated with filament bending. The WLC model subjects the statistical ensemble to the constraints

$$L_c x = \int_0^{L_c} ds \left( \frac{d\mathbf{r}}{ds} \right) \text{ and } \left( \frac{d\mathbf{r}}{ds} \right)^2 = 1, \quad (2)$$

which ensure that the ends of the chain have separation  $x = R/L_c$  and that the chain is locally inextensible. The path integral of the partition function is difficult to evaluate analytically due to the constraint of local inextensibility, and explicit solutions are typically found in the limit of flexible<sup>14,15</sup> and stiff<sup>16,17</sup> chains, and it is only very recently that an analytical solution has been found in ref. 18. However, a simplified solution can be found for chains of any stiffness if a mean field approach is used to relax the constraint of local inextensibility to the one of global inextensibility.<sup>19</sup> The result is a partition function in the form of a single-variable integral, which can be solved analytically in two dimensions. In three dimensions, however, it must be solved numerically, and a compact interpolation of an exact numerical solution of the partition function leads to the free energy of a single filament of the form<sup>19</sup>

$$F(x) = \frac{A\pi^2}{2L_c} (1 - x^2) + \frac{2(k_B T)^2 L_c}{\pi A (1 - x^2)}, \quad (3)$$

where the bending stiffness is proportional to the persistence length *via*  $A = k_B T L_p$ . There are clearly two competing terms, the first of which is at a maximum when  $x = 0$  and the second of which is at a maximum when  $x = 1$ . The equilibrium end to end

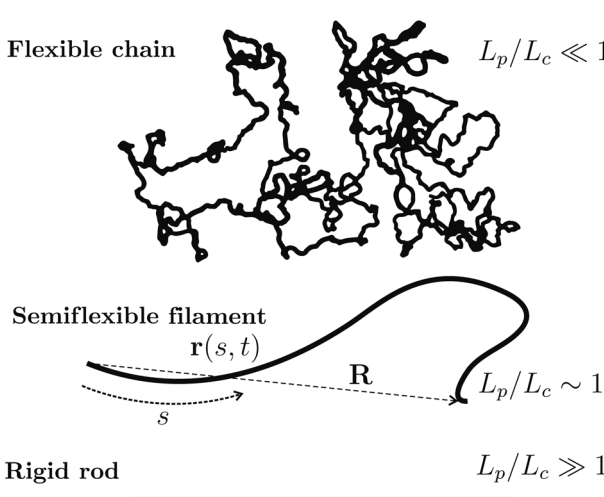


**Fig. 1** Chain conformation depends on persistence length,  $L_p$ , and contour length,  $L_c$ . Flexible chains take a random coil formation, semiflexible filaments are comparatively straight with thermally induced bending undulations, and rigid rods are not influenced by thermal energy.

distance is found by minimising the free energy with respect to  $x$ , leading to

$$x_0 = \sqrt{1 - 2L_c/L_p\pi^{3/2}}. \quad (4)$$

This defines the rest length of a semiflexible filament under no force. When  $L_p/L_c < 2/\pi^{3/2}$  there is no solution for the end to end distance, and the chain will take a more entropy-driven random coil conformation.

## 2.1 Equilibrium stretch and compression

For many biological filaments,  $L_p/L_c$  is greater than one; their persistence lengths are typically large, and when filaments form crosslinked networks, the effective contour length becomes the separation between crosslinks.<sup>20</sup> For such filaments, or when the filament is subject to a large extension force,  $x$  is close to unity and the approximation  $1 - x^2 \approx 2(1 - x)$  is valid. Applying this to eqn (3) and differentiating with respect to the true end to end separation,  $xL_c$ , we find the approximate force-extension relationship for an inextensible filament:

$$f(x) \approx -f_c + \frac{(k_B T)^2}{\pi A(1-x)}, \quad (5)$$

where  $f_c = A\pi^2/L_c^2$  is a constant, equivalent to the classic Euler buckling force of a pinned filament of bending modulus  $A$  and length  $L_c$ .<sup>21</sup> As the filament is stretched to its full length, the force (5) will of course diverge as a consequence of inextensibility. In reality, the filament length can be stretched by force and the extensibility needs to be taken into account. For the simple case, when the filament is subject to a force  $f$ , the contour length can be expected to increase as  $L_f = L_c + f/k_m$ , where  $k_m$  is the mechanical spring constant of filament stretching defined as  $k_m = (Y/L_c)\int dS$ .  $Y$  is the Young's modulus which is assumed to be strain independent; it should be noted that the  $L_p$  and  $Y$  are not unrelated in continuum elasticity, as  $k_B T L_p = A = IY$ , where  $I$  is the filaments' moment of inertia.<sup>21</sup> Accounting for an extensible contour length,  $L_f$ , and using eqn (5) yields

$$x(f) = \left(1 + \frac{f}{k_m L_c}\right) \left(1 - \frac{k_B T}{\sqrt{\pi A(f+f_c)}}\right). \quad (6)$$

It should be pointed out that this formula differs from the original publication<sup>19</sup> due to a typing error. This was noted by Holzapfel and Ogden, where they found the corrected formula to agree well with single actin filament extension experiments.<sup>22</sup> Fig. 2 shows force extension for filaments under tension using the persistence length of actin and eqn (6). At vanishing force, where the curves meet the  $x$ -axis, the  $x$  value coincides with  $x_0$ , the filaments' rest length defined by eqn (4). When  $x$  approaches one, all filaments stiffen, as it becomes more difficult to overcome thermal undulations. Beyond  $x = 1$ , the filaments are taut and begin to stretch, exhibiting linear enthalpic elasticity.

As filaments will not only be under tension, their response to compression must also be considered. Under a constant compressional force, which is parallel to the end to end vector

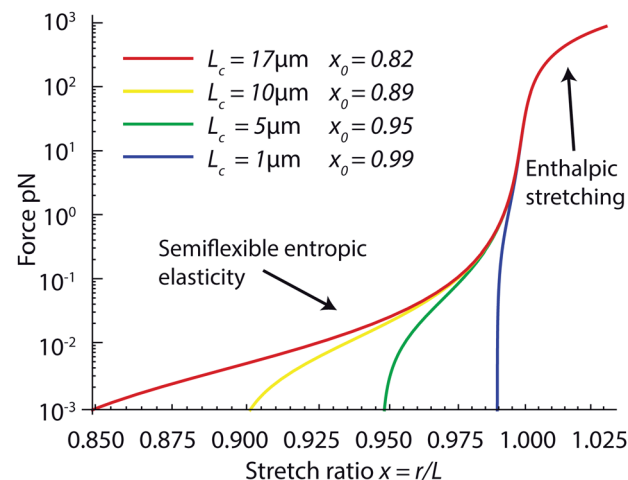


Fig. 2 Logarithmic force-extension plots for extensible filaments using eqn (6). Parameters correspond to those of an actin filament of  $L_c = 1 \mu\text{m}$ ,  $5 \mu\text{m}$ ,  $10 \mu\text{m}$ , and  $17 \mu\text{m}$ ,  $L_p = 17 \mu\text{m}$ ,  $Y = 2 \text{ GPa}$ , and filament diameter  $d = 7 \text{ nm}$ .

of the filament, the work done is  $\Delta W = f \cdot L_c x$ . The full free energy (eqn (3)) including the work term is plotted in Fig. 3 for increasing compressive force. When the force is equivalent to the Euler critical force (the buckling force of an elastic rod,  $f_c$ ), the free energy minimum is at the origin and the filament is always buckled. For a non-zero force smaller than  $f_c$ , there are two energy minima. This indicates that if the compression is great enough, there will be a phase transition, with the filament able to switch from an unbuckled state to a buckled state. As this is a thermal system, the free energy barrier between states need only to be  $\sim k_B T$  for a filament to buckle.

## 2.2 Dynamic deformation

While the equilibrium response is useful, it deals with the limit of quasi-static deformations which will clearly not be the case in

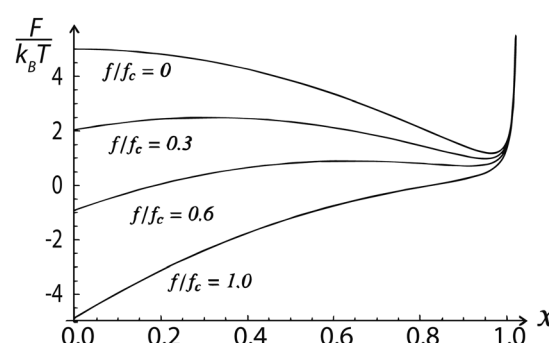


Fig. 3 Plots of the free energy,  $F(x)$  (see eqn (3)), for a typical semi-flexible filament ( $A/k_B T L_c \equiv L_p/L_c = 3$ ) under increasing compressive force  $f$  measured in units of the Euler critical force  $f_c = A\pi^2/L_c^2$ . There are four regimes:  $f/f_c = 1$  there is one minimum and the filament is buckled; between  $f/f_c = 0.6$  and  $f/f_c = 0.3$  there are two coexisting minima and there is a critical value of  $x$  where the filament switches between resisting compression and buckling;  $f/f_c = 0$  there is one minimum where the filament is unbuckled.<sup>23</sup>

many practical situations, particularly those in biology. In this section, we look briefly at the classical dynamics of the worm-like chain; for a thorough discussion of WLC dynamics see ref. 24. The filaments discussed here may be considered as isolated in solution, and chain interactions will be discussed in the later section on networks.

If a semiflexible chain is weakly bending, the dynamics of transverse deviations follow the Langevin equation:<sup>24,25</sup>

$$\gamma_{\perp} \frac{\partial \mathbf{r}_{\perp}}{\partial t} = -A \frac{\partial^4 \mathbf{r}_{\perp}}{\partial s^4} + f \frac{\partial^2 \mathbf{r}_{\perp}}{\partial s^2} + \xi_{\perp}, \quad (7)$$

where  $\mathbf{r}_{\perp}(s,t)$  is the transverse displacement at filament arc length  $s$  (see Fig. 1) at time  $t$ .  $\gamma_{\perp}$  is the solvent friction per unit length,  $\xi_{\perp}(s,t)$  is the Gaussian thermal noise, and as before,  $A$  is the bending rigidity. The solution to eqn (7) is given in the form of an infinite series:

$$\begin{aligned} \mathbf{r}_{\perp}(s, t) &= \sum_{n=1}^{\infty} \mathbf{a}_n(t) \sqrt{\frac{2}{L_c}} \sin(k_n s), \\ \langle \mathbf{a}_n(t) \mathbf{a}_m(0) \rangle &= \delta_{mn} \langle \mathbf{a}_n^2 \rangle \exp(-t/\tau_n), \end{aligned} \quad (8)$$

where  $k_n = n\pi/L_c$  are the eigenvalues and  $\mathbf{a}_n(t)$  is the time dependent amplitude of each mode. The correlation between amplitudes after time  $t$  is such that the eigenmodes relax independently and exponentially, with relaxation constants  $\tau_n$ . The mode amplitudes and decay constants using equipartition theorem are found to be  $\langle \mathbf{a}_n^2 \rangle = 2k_B T / (Ak_n^4 + fk_n^2)$  and  $\tau_n = \tau_1 / (n^4 + n^2 f/f_c)$ , where as before  $f_c = A\pi^2/L_c^2$  is the Euler buckling force of the longest mode and  $\tau_L = \gamma_{\perp} L_c^4 / A\pi^4$  is the relaxation constant of this longest mode.

One way to relate eqn (8) to a measurable quantity is to calculate the mean squared transverse displacement (MSD) of the filament:  $\delta r_{\perp}^2(t) = \langle [\mathbf{r}_{\perp}(s, t) - \mathbf{r}_{\perp}(s, 0)]^2 \rangle$ . This can be measured directly by dynamic light scattering,<sup>26</sup> or indirectly using passive and active microrheology methods.<sup>27</sup> To relate the MSD to a more representative material property, such as the dynamic shear modulus, the linear susceptibility  $\alpha^*(\omega)$  must first be calculated. The complex part of  $\alpha^*(\omega)$  is related to the MSD power spectrum,  $\delta r_{\perp}^2(\omega)$ , via  $\alpha''(\omega) = -\delta r_{\perp}^2(\omega) / 2k_B T$ . The full linear susceptibility can then be found using the Kramers-Kronig relations, which relate the real and complex parts of response functions, leading to

$$\alpha^*(\omega) = \frac{L_c^3}{k_B T L_p \pi^4} \sum_{n=1}^{\infty} \frac{1}{(n^4 + n^2 f/f_c)(1 + i\omega\tau_n)} \quad (9)$$

Typically, the dynamic shear modulus as determined by microrheology is related to the linear susceptibility *via* the relation  $g^*(\omega) \propto 1/\alpha^*(\omega)$ , where the proportionality constant depends on the microrheological technique.<sup>28</sup> Here, the lower case  $g$  is used for the shear modulus because it differentiates the microrheological modulus from the full shear modulus: the full modulus will take into account the solvent properties, and for high frequencies it is theoretically predicted that  $G^*(\omega) = (1/15) l_c \rho \alpha(\omega) - i\omega\eta$ , where  $l_c$  is the distance between entanglements,  $\rho$  is the filament number density, and  $\eta$  is the solution viscosity.<sup>29,30</sup> The  $\rho l_c$  term accounts for the viscoelastic contribution of single filaments per area and  $i\omega\eta$  accounts for the

solvent inertia. The high frequency limit of  $g^*$  is proportional to  $\omega^{3/4}$ , which is also predicted by other theories.<sup>29,31</sup> Examples of the high frequency power law can be observed in experiments on actin solutions<sup>28,30,32,33</sup> and microtubules.<sup>34</sup> The application of force alters the power-law exponent, and will decrease it from 3/4 to lower limit of 1/2 at large tension.

### 3 Filamentous networks

In this section, we take the mechanical properties of single filaments outlined above and examine the mechanical properties that occur when they form networks. The mechanical properties of a network arise from the organisation and behaviour of its constituent filaments and crosslinks.<sup>35</sup> As the mechanical properties of single filaments are already understood, we will first briefly examine the three standard types of crosslinks: the pin joint, the rotating joint, and the weld joint. Pin joints transmit no bending moments between incident filaments, only allowing axial forces; these usually correspond to connections in flexible polymer networks, but may also describe the mating of semiflexible or rigid filament ends with a flexible crosslinker. Rotating joints describe the pinning of semiflexible filaments or rigid rods with a flexible linker, such that bending moments are transmitted along each filament but they freely rotate with respect to each other. Finally, there is a weld joint, where bending moments are transmitted between incident filaments and there is an energy penalty when rotating with respect to each other. These three are considered as “ideal” crosslinks, and sometimes it may be necessary to make modifications to account for the crosslinkers’ own mechanical response, such as in actin networks crosslinked with the compliant protein filamin-A.<sup>36–38</sup> An important issue with respect to the dynamic response is how stable the crosslink is. In many biological situations, crosslinks are not covalently bonded and may dissociate and re-form at a characteristic rate. In the following discussion, we define permanent crosslinks as those that have no time-dependent evolution.

#### 3.1 Central force networks

Before discussing the mechanical properties of networks, it is worth considering whether or not we even have a network in the first place. There are two defined stages of network formation, namely, geometric percolation and stiffness percolation. Geometric percolation occurs when every filament is connected to each other in some way, *i.e.*, there is a path through the network to navigate between crosslinks. Stiffness percolation, sometime called the point of marginal stability,<sup>39</sup> occurs when the modulus of the network at zero strain is non-zero. Typically, stiffness and geometric percolation are distinct events, as just because a network is geometrically connected it does not mean that stresses can be supported throughout the network. The exception to this occurs in weld jointed networks: recent work shows that stiffness percolation can come close to geometric percolation when a fraction of rotating joints are replaced with weld joints.<sup>40</sup> A critical factor in determining network stiffness is the average coordination number,  $\langle z \rangle$ , where  $z$  is given by the

number of incident filaments at a crosslink. It was first shown by Maxwell that networks formed with pin joints (so called central force networks) require a minimum  $\langle z_c \rangle$  of  $2d$  to be stable, where  $z_c$  is the critical coordination number and  $d$  is the number of spatial dimensions.<sup>41</sup> In central force networks, forces can only be transmitted axially and consequently, filaments only contribute to elasticity through their stretch modulus,  $\mu$ , where  $\mu = Y \int dS$ .

It is clear that for crosslinks between filaments (where  $\langle z \rangle = 4$ ) rigidity will only be reached with pin joints in two dimensions. As biological networks are typically in three dimensions, where  $\langle z \rangle$  must be greater than 6 for central force rigidity; there are clearly other factors involved. Interestingly, rubber networks, which are aptly described by pin joints due to their inherent flexibility, have an apparent non-zero modulus for  $\langle z \rangle$  as low as 3. Theories of rubber elasticity circumnavigate the issue by the implicit assumption of affine deformation at the network edge (*i.e.* the network deforms locally as the macroscopic applied deformation), which assumes that the network is already stiff. However, it is often unnoticed that rubbers never truly see the end of their shear modulus relaxation. This is frequently overlooked due to the very slow relaxation at long times (tens of years), thus not typically noticeable on  $G'$  vs.  $t$  and  $\log[G']$  vs.  $\log[t]$  relaxation plots, with the appropriate scaling being  $G'$  vs.  $\log[t]$ .<sup>42,43</sup> As to whether there is true equilibrium is up for debate; however, recent work shows that affine elasticity can be recreated as long as there is a finite bending modulus, no matter how weak, so long as the network chains are very long.<sup>44</sup>

### 3.2 Origins of network rigidity

Rubbers aside, there are primarily two ways for networks with freely rotating crosslinks to transit to a finite shear modulus: the most commonly noted is to account for the bending modulus and the other is to consider prestress.<sup>44–46</sup> More recently it has been shown that adding crosslinkers which have a finite energy cost when two filaments rotate with respect to each other can also rapidly promote network stability.<sup>40</sup> In simulations on three dimensional filament networks with coordination numbers below the critical value of 6, it is found that for any finite bending modulus,  $A$ , there is a finite shear modulus at zero strain.<sup>44–46</sup> Once the network is stable, the small-strain elasticity can either arise from the bending or the stretching of filaments, determined by the ratio of  $A/\mu$ , where  $\mu$  is the stretch modulus (equivalent to  $k_n L_c$ ). The coordination number also plays a role, as when  $z$  becomes much larger than  $z_c$ , the network is highly constrained and elasticity primarily arises from the stretching of filaments.<sup>45</sup> For networks of coordination 4, typical of biological networks and the crosslinking of filaments, it is found that when  $A/\mu \ll 1$ , the initial modulus depends on  $A$ , and when  $A/\mu \gg 1$  the initial modulus depends on  $\mu$ ;<sup>45</sup> unsurprisingly, deformation will occur *via* the mode of least resistance. Pre-stress, or applied strain, can also induce a rigidity transition for central force networks, which may be thought of as aligning geometrically connected elements to stretch such that they become taut. Simulations on isotropic,

affinely deformed networks show that in this case the modulus increases as  $G \sim \{\text{strain}\}^2$ .<sup>46</sup> The two effects are not independent, and can work together to give network stiffening. For a network that was initially stiff as a consequence of bending, pre-stress can initiate a strain-stiffening response as filaments align with the strain and begin to stretch, resulting in a stretch-bend coupled modulus which at large strains will be dominated by stretching.<sup>45,46</sup>

Another consideration for a network under strain is whether it deforms affinely or nonaffinely, as well as the consequences of each type of deformation. If a network deforms affinely, any local region will deform identically to the macroscopic deformation, whereas for nonaffine deformation local regions may deform in any fashion to achieve local mechanical equilibrium, so long as when all the regions are taken together the macroscopic deformation is recovered. All networks must be nonaffine at some scale, because they are made of discrete elements; however, it becomes apparent that if the length scale of nonaffine deviations is not much larger than the mesh size, the network can be said to deform in an approximate affine manner. Full discussion of nonaffinity can be found in ref. 47, but in general nonaffinity will lower the shear modulus when compared to affine deformation, as there are fewer constraints on how the material must deform internally.<sup>35,46</sup> In the case of semiflexible filaments, deformation can be either affine or nonaffine depending on the network structure and the level of strain (see Fig. 4).

Fig. 4 shows a ‘phase diagram’ of types of network elasticity as a function of filament length and density, for 2D networks of  $\langle z \rangle = 4$ . In other words, the diagram illustrates the changes in elasticity that occur for semiflexible filaments with varying length and density of filaments. At low densities and short lengths, a network cannot form due to insufficient cross-linking, leaving a solution of filaments. Above a certain density

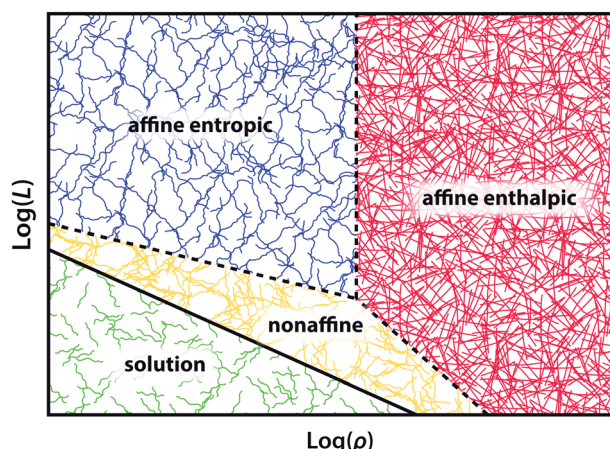


Fig. 4 Phase diagram adapted from ref. 48, showing the prevailing mode of elasticity and the network structure as a function of length and density for a fixed persistence length. At low densities and lengths, the network is in solution, which gains marginal stability above a critical density and length. At longer lengths and intermediate density, the network deforms affinely and elasticity is dominated by the entropic stretching of filaments. At high densities, the network is dominated by enthalpic bending and stretching of the network.

and length, percolation occurs and the network gains stability. In the 2D network this stability will occur even for central force networks, but for a 3D network the finite modulus is solely a result of the extra constraints provided by bending.<sup>44</sup> In either case, the network is nonaffine and the elasticity is dominated by filament bending (see Table 1); however, for a ratio of  $A/\mu \gg 1$ , this elasticity will be dominated by filament stretching.<sup>44,48,49</sup> At longer lengths and lower densities, the network changes to an approximately affine regime, where the separation between crosslinks is large enough for entropic elasticity to dominate. As the filaments are semiflexible, strain stiffening occurs, where for permanent crosslinks the shear modulus increases with applied pre-stress,  $G \sim \sigma^{3/2}$ .<sup>50</sup> When the density is high enough, the distance between crosslinks is too short for entropic elasticity to play a role and enthalpic stretching dominates. If  $A/\mu \gg 1$ , the affine enthalpic regime will experience linear elasticity arising from the stretching modulus; however, if  $A/\mu \ll 1$ , the affine enthalpic network will show strain stiffening as the network switches from enthalpic bending to enthalpic stretching. The theoretically predicted initial moduli for each of these regimes are shown in Table 1, valid for permanent flexible crosslinks between semiflexible filaments. However, one must be clear that the response can be greatly modified by changing the type of crosslink and its permanence.<sup>51</sup> That being said, there is often a degree of redundancy in the mechanical response where, for example, adding angle constraining crosslinkers to a free rotating crosslinked semiflexible network can enact a similar response to changing filament density.<sup>40</sup>

### 3.3 Network dynamics

We will now consider the dynamics of networks formed from semiflexible filaments; this can be a question arising in the simple case of steric interactions in semidilute solutions to the more complicated situations such as networks formed with transient crosslinks between filaments. The dynamics of a network stem from that of single filaments and their interactions, and it is anticipated that the exact network geometry and heterogeneity does not alter the qualitative nature of network dynamics, only the coefficients.<sup>54</sup> The effects of interactions, such as crosslinking, steric interactions, and interactions with non-network species, can be accounted for with two extensions to the WLC model discussed in Section 2.2, specifically by modifying the filament relaxation modes in eqn (8). The first

**Table 1** Theoretical predictions for the shear modulus of various network types.  $\rho$  is the filament density,  $\xi$  is the mesh size, and  $\sigma_c = k_B T L_p / L_c^2 \xi^2$ .<sup>a</sup> If  $A \ll \mu$  then there will be a transition from bending dominated elasticity to enthalpic stretching elasticity at larger strains

Regime	$G'_0$	Prestress	Ref.
Solution	0	Const	
Nonaffine	$A/L_c^4$	Const	44,48,50
Rubber	$k_B T \rho$	Const	52
Affine entropic	$A^2/k_B T \xi^2 L_c^3$	$G_0(1 + \sigma/\sigma_c)^{3/2}$	19,50,53
Affine enthalpic	$A/L_c^4 \rightarrow a$	$4\mu/\xi^2$	44,48

extension leads to the ‘glassy worm-like chain’ model (GWLC) and deals with the slowdown or stretching of relaxation as a consequence of interactions,<sup>25,26,54</sup> and the second extension leads to the ‘inelastic glassy worm like chain’ model (iGWLC), a modification to the GWLC that deals with the consequences of time dependent crosslinking.<sup>54–57</sup>

The glassy wormlike chain, so-called from its analogy to soft glassy materials,<sup>58,59</sup> follows from a simple exponential stretching of the WLC relaxation spectrum in eqn (8). The stretch of relaxation times is defined by an effective Boltzmann factor,  $\exp(\varepsilon)$ , where  $\varepsilon$  is the characteristic energy (in units of  $k_B T$ ) of interactions that must be overcome to induce a conformational change. As interactions are distributed spatially along the filament (*e.g.*, steric interactions or crosslinking), it stands to reason that modes of a longer wavelength will be inhibited by a proportionally greater number of interactions, and modes shorter than a critical wavelength will experience no interactions. Consequently, the WLC relaxation spectrum is modified to

$$\tau_n \rightarrow \tilde{\tau}_n = \begin{cases} \tau_n & (\lambda_n < A) \\ \tau_n \exp[\varepsilon(\lambda_n/A - 1)] & (\lambda_n \geq A) \end{cases} \quad (10)$$

where  $A$  is the average separation between interactions, and the number of interactions above  $A$  increases as  $(\lambda_n/A - 1)$ . Substituting the GWLC relaxation spectrum into eqn (9) gives the linear susceptibility, and correspondingly, the microrheological modulus,  $g^*$ . The real and imaginary parts of  $g^*$ , evaluated at zero tension, are shown in Fig. 5 for increasing values of  $\varepsilon$ .

For both  $g'$  and  $g''$ , there are two distinct power-law regimes, one at low frequencies and one at high frequencies, with the transition occurring at  $\sim \omega_A = 2\pi/\tau_A$ . The high-frequency power law is simply that of the single filament response and goes as  $\omega^{3/4}$ . The low-frequency power law is a consequence of the exponential stretching, and its exponent

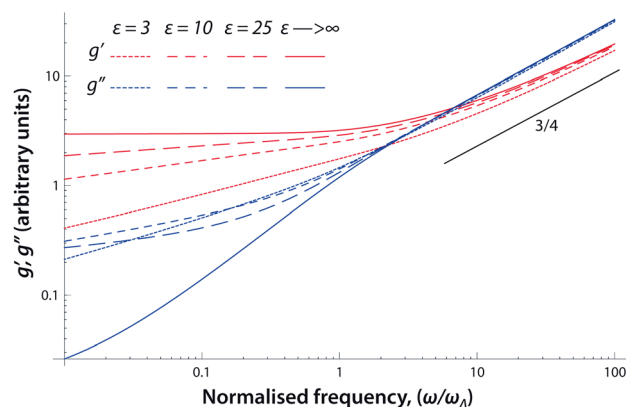


**Fig. 5** The frequency dependence of the real and imaginary parts of the GWLC microrheological modulus,  $g'$  and  $g''$ , respectively, where  $g^* \propto 1/\omega$  at  $f = 0$  for increasing interaction energy. The plots are calculated using eqn (9) with the modified relaxation spectrum from eqn (10). The x-axis is scaled by  $\omega_A = 2\pi/\tau_A$ , where  $\tau_A$  is the relaxation time corresponding to the mode of wavelength  $A$ , *i.e.* the smallest mode to ‘feel’ interactions.

is a function of the interaction energy  $\varepsilon$ , pre-stress  $f/f_c$ , and relaxation constant  $\tau_L$ . The exponent of the  $g'$  low-frequency power law,  $\omega^\beta$ , positions the filament on a continuous scale between the states of purely elastic, with  $\beta = 0$ , and purely viscous, with  $\beta = 1$ . As the interaction energy increases, the exponent decreases and the network becomes effectively more elastic. At the limit of  $\varepsilon \rightarrow \infty$ , the interactions correspond to permanent crosslinks and the network becomes purely elastic at low frequencies until the transition to the high frequency regime, as is observed in experiments on permanently cross-linked actin.<sup>30,60</sup> The low-frequency power law of the loss modulus  $g''$  does not increase monotonically with increasing interaction energy as in the case of  $g'$ . Initially,  $g''$  will see a decrease in power law and increase in magnitude with interaction energy, but as  $g'$  approaches a power-law exponent of 0 and the network becomes more elastic, the magnitude of  $g''$  will begin to decrease and the power-law exponent will increase. This can be visualised as each particular network sitting on a specific point of a phase transition scale between purely liquid and purely elastic states, with the change of exponent  $\beta$  reflecting a change in this position.

The effects of pre-stress are more complicated, and can either result in strain stiffening or strain softening depending on the strength of the interaction. It is expected that an applied tension will assist the filament in overcoming interactions such that the effective interaction energy is  $\varepsilon \rightarrow \varepsilon \pm f/f_\perp$ , where  $f_\perp$  represents the scale of thermally induced force fluctuations. In the absence of this tilting, pre-stress will lower the exponent and increase the shear modulus resulting in strain stiffening; however, with the force-induced lowering of the barrier  $\varepsilon$ , this will eventually be over-compensated and the network will soften. Consequently, networks present a scale of stress stiffening depending on the value of  $\varepsilon$ , and such behaviour is indeed observed in experiments on actin.<sup>26,61</sup> In the limit of permanent crosslinks, corresponding to  $\varepsilon \rightarrow \infty$ , strain stiffening goes as  $\propto \sigma^{3/2}$ , examples are seen in experiments<sup>50</sup> and predicted by other theories as well.<sup>19</sup> In addition, as with single filaments, pre-stress will slightly lower the exponent of the high frequency power, with the lower limit being  $\omega^{1/2}$ . This effect is observed in actin filaments prestressed with myosin II.<sup>33</sup>

The inelastic glassy wormlike chain (iGWLC) is a further modification of the GWLC model. iGWLC is designed to account for transient crosslinks, in particular for those seen in cytoskeletal networks.<sup>55,56,62</sup> The principle of iGWLC is to allow the separation  $\lambda$  between interactions to evolve in time, simulating the breaking or reforming of crosslinks. The results of the iGWLC are succinctly expressed by the constitutive diagram shown in Fig. 6, and will also be discussed later in the context of cells.

The key result of the iGWLC is the description of network fluidisation, which arises from the transient nature of the crosslinks: when the strain rate is low, crosslinks can break and re-form during the time scale of strain; however, if a large strain is applied quickly, large stresses can build up in the network as crosslinks have no time to unbind kinematically. Consequently, the large stresses are enough to overcome the majority or

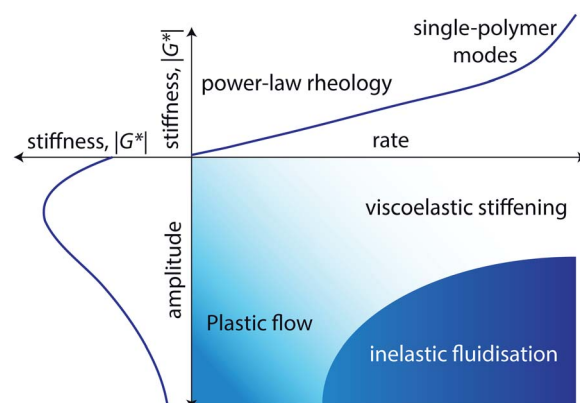


Fig. 6 Constitutive diagram for the iGWLC model, adapted from ref. 56. The top panel demonstrates the low and high frequency power law modulus, similar to those shown in Fig. 5. The central panel illustrates the mechanical response to oscillatory shear as a function of frequency and strain amplitude: at low amplitudes and frequency, the response is approximately linear; at low frequencies and high strain the network exhibits plastic flow as crosslinks begin to break; and at high frequencies and strain, fluidisation occurs. In the quasistatic regime (left panel), there is strain stiffening at low amplitudes due to entropic stiffening individual chains, but at high amplitudes (and stress) there is strain softening as interactions (e.g. crosslinks) are more readily overcome.

crosslinks and the network fluidises. This is followed by a period of recovery as crosslinks begin to reform.

## 4 Cytoskeleton and its constituent networks

In this section, we take the concepts of filaments and networks from the previous sections and see how they can be applied to the cell cytoskeleton, as well as *in vitro* networks formed by cytoskeletal filaments. The cytoskeletal network and its varying regional specialisation are constructed from three types of filaments: actin filaments (sometimes called microfilaments), microtubules (MTs), and intermediate filaments (IFs). All three are remarkably stiff in comparison to synthetic polymers, which is illustrated by their large persistence lengths: microtubules  $L_p > 1$  mm, actin filaments  $L_p \sim 17$   $\mu\text{m}$ , and intermediate filaments  $L_p \leq 1$   $\mu\text{m}$ ; consequently, they behave in a semiflexible manner. Cytoskeletal networks are highly dynamic structures and will reorganise themselves in response to external stimuli (mechanical or biochemical). This process can be rapid, for example the whole actin cortex can be reassembled in a matter of minutes.<sup>63,64</sup> The particulars of the network formed are determined by their associated proteins (for example, actin has over 150 discovered so far<sup>6</sup>), which control assembly, disassembly, and filament interactions (e.g. crosslinking).<sup>10</sup>

### 4.1 Protein filaments in cytoskeleton

**Actin filaments.** Actin filaments are constructed from globular-actin (G-actin), and may be regarded as two parallel protofilaments wound together in a right handed helix of diameter

8 nm. Through interactions with the associated proteins, actin can form a range of structures suited to different functions. These include isotropic networks, branched networks, bundled networks, and stress fibers (with myosin II), see Fig. 7. Depending on their organisation and the type of crosslink, they can resist notable compressional forces, in addition to tensional force. Actin filaments are polar, allowing myosin heads to 'walk' in a preferential direction along their axis, a process that has recently been videoed with a high speed atomic force microscope.<sup>65</sup> The interaction of actin networks with myosin molecular motors can reshape the network and generate tension.<sup>6,10,66</sup> In the past decade there has been great progress in controlling the structures formed with actin by using purified actin associated proteins.<sup>33,50,67–71</sup> More recently, work has been carried out to create higher order actin structures: Reymann *et al.* built structures such as concentric contractile rings formed by tailoring the position of actin nucleation sites,<sup>72,73</sup> and other work has resulted in a complete actin cortex being reconstructed inside a liposome.<sup>74</sup>

**Intermediate filaments.** Intermediate filaments are the softest, most extensible of the cytoskeletal proteins, and at present the molecular mechanisms governing their assembly and disassembly are largely unknown.<sup>75</sup> Originally, they were named intermediate filaments due to their diameters being typically around 10 nm, placing them between actin filaments and microtubules. They are believed to have highly tissue-specific functions, with varying cells expressing different IFs (*e.g.* keratin in the epithelial cells and vimentin in the mesenchymal cells). Generally, they may be separated into two

classes: those that are situated in the cell nucleus and those that occupy the cytoplasm. Only metazoan cells exhibit both types of IFs; insects only express nuclear IFs, and plants and fungi express neither, which is believed to be a consequence of the cell wall.<sup>76</sup> This is in contrast to actin filaments and microtubules, which are present in all eukaryotes and are highly conserved between species (*i.e.*, the protein sequence differs little between species). IFs play an integral role in the mechanical integrity of epithelial cells, in which IF networks of individual cells are connected *via* transmembrane proteins called desmosomes to adjacent cell networks.<sup>77</sup> Epithelial IF networks undergo continuous cyclic assembly and disassembly, where filaments nucleate near the cell edge and move towards the nucleus bundling and forming networks as they approach; some fibers will join a more permanent IF network surrounding the nucleus, whereas others will disassemble to be recycled.<sup>75</sup> In the cytoplasm, intermediate filaments are known to contribute greatly to strain stiffening at large extensions, which is thought to protect cells from over-extension.<sup>78,79</sup> In the nucleus, intermediate filaments called lamins form the nuclear lamina, a meshwork primarily seated under the nuclear envelope providing mechanical support, which leads to the nucleus being typically 5–10 times stiffer than the surrounding cytoplasm.<sup>9</sup>

**Microtubules.** Microtubules are the stiffest of the cytoskeletal filaments, with persistence lengths so large that they remain relatively straight even when spanning large regions of the cell.<sup>11</sup> The persistence length of microtubules is not constant and can vary dramatically depending on the contour length, where  $L_p = 110 \mu\text{m}$  for filaments of  $L_c = 2.6 \mu\text{m}$ , increasing to  $L_p = 5 \text{ mm}$  for  $L_c = 47.5 \mu\text{m}$ .<sup>80</sup> As microtubules often span the length of the cell, their persistence lengths are typically above 1 mm. Microtubules are tubular structures of diameter 25 nm formed of  $\alpha$ -tubulin/ $\beta$ -tubulin dimers, and in the cell, typically have one end attached to a centrosome near the cell nucleus. The free end goes through stages of rapid growth and disassembly in a process called dynamic instability, allowing them to rapidly probe intracellular space.<sup>81</sup> As with actin filaments, microtubules are polar and will interact with molecular motors (kinesins and dyneins); however, in contrast to actin filaments, these molecular motors do not reorganise microtubules directly and only use them as intracellular highways to shuttle cargo.<sup>82</sup> Microtubules will resist compressional forces, and their presence significantly alters the mechanical response of *in vitro* actin networks by constraining the response of actin<sup>83</sup> and creating a fiber reinforced gel.<sup>84</sup> This causes the actin networks to stiffen and gives rise to a more pronounced nonlinear rheology.<sup>85</sup> The interaction of MTs with intermediate filaments considerably increases the compressional forces they can withstand before buckling.<sup>86,87</sup> This is due to intermediate filaments acting as braces for microtubules, allowing bending modes to exist at higher modes beyond the first. Compressional energy is then spread out between modes, and consequently, buckling will occur at a larger compressional force.<sup>88</sup>

The cytoskeleton is coupled to the environment through integrins and cadherins, transmembrane proteins that bind to the extracellular matrix (ECM) and other cells, respectively. The cadherin protein, desmosome, which has been mentioned

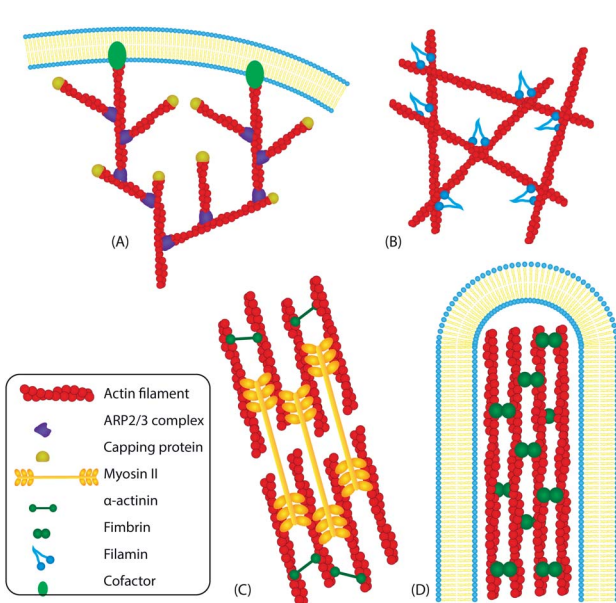


Fig. 7 Actin cytoskeletal networks: (A) branched networks form with the ARP2/3 complex oriented towards the membrane, and crosslinks maintain an angle of 70°. (B) Random network crosslinking with flexible and extensible filamin crosslinker. (C) Stress fibers formed with long orthogonal  $\alpha$ -actinin crosslinks with parallel myosin II bundles. (D) Bundled network formed with small orthogonal fimbrin crosslinks, together they form stiff filopodia protrusions.

previously, connects the intermediate filaments of epithelial cells together giving structural integrity to epithelial tissue. Both cadherins and integrins are capable of binding to actin through adapter proteins which leads to cytoskeletal remodelling. The binding of integrins can lead to the formation of focal adhesions, large protein complexes that mediate force transmission, which can resist forces up to 100 nN.<sup>89</sup> This force level is much higher than that of a single fibronectin integrin which can withstand only 1–2 pN.<sup>90</sup> Focal adhesions transmit forces between the ECM and the cytoskeleton, but it is observed that if the ECM is not rigid, focal adhesions fail to mature,<sup>91</sup> indicating the importance of the cell environment on the cytoskeletal structure. For an in-depth review of focal adhesion complexes see ref. 89.

#### 4.2 Cytoskeletal networks *in vitro* and *in vivo*

In this section we focus on the mechanical properties of actin networks formed *in vitro* and *in vivo*, as they are the most heavily researched and show the widest range of structures of all the cytoskeletal proteins. Fig. 7 shows schematics of several actin networks in the cell, with their associated crosslinkers.

Early work on the mechanics of actin networks used irreversible crosslinkers, rather than dynamic cytoskeletal crosslinkers, so as to focus on the response of actin filaments. These networks often have distances between crosslinks comparable to the persistence length and as such the filaments behave semiflexibly. At low crosslinking densities, linear elasticity is observed corresponding to the nonaffine bending region in Fig. 4. Beyond a critical crosslinking density, the network changes to the affine entropic region and strain stiffening behaviour is observed where  $G' \propto \sigma^{3/2}$ ,<sup>50</sup> as described by the GWLC model. The power-law rheology of permanently cross-linked networks follows that of the GWLC with infinite interaction energy (see Fig. 5), which represents permanent crosslinks by making the interaction between filaments insurmountable. This leads to an observed plateau of  $G'$  at low frequencies, implying a purely elastic network, and an  $\omega^{3/4}$  power law at high frequencies resulting from the individual filament response.<sup>30</sup>

Networks constructed by actin filaments and filamin form a loose gel of orthogonal filaments at incredibly low crosslinking densities. Filamin is a large flexible cytoskeletal protein (persistence length of 20 nm) which preferentially crosslinks filaments at approximately 90° to each other (see Fig. 7B). In addition, filamin crosslinks are transient and have a dissociation rate constant of  $K_{\text{off}} \sim 0.6 \text{ s}^{-1}$ .<sup>92</sup> In contrast to irreversible crosslinks, this leads to the observed power law fluid rheology (see GWLC) with a low frequency power law of  $\omega^{0.17}$ .<sup>62,71</sup> With a greater increase in crosslinking, the network becomes more elastic and it leads to a lower value of power-law exponent. This effect is equivalent to decreasing  $A$  in eqn (10). Pre-stress has a similar effect of decreasing the power-law exponent and increasing the modulus,<sup>62,68</sup> highlighting the levels of redundancy in tuning the power law rheology and modulus of these networks. However, unlike permanently crosslinked networks, the stress stiffening exponent is less than 3/2 and will increase

approximately linearly,<sup>62</sup> as discussed in the section on GWLCs above. Above a critical filamin concentration, it has been found that filamin induces the formation of actin bundles, increasing the bending stiffness and yield stress.<sup>93,94</sup> This shifts the network away from entropic strain-stiffening into the regime of enthalpic bend stretch strain-stiffening. Qualitatively, the rheological properties see little change, but there is a corresponding decrease in the power-law exponent as the networks become stiffer and more elastic. Pre-stress in actin networks does not have to come externally. *In vitro* experiments have shown that networks can be prestressed internally *via* interactions with non-muscle myosin II,<sup>28,66,68</sup> or by self generated pre-stress during polymerisation.<sup>95</sup> *In vitro* contracted actomyosin gels also increase their modulus and lower their frequency response substantially with internally generated prestress.<sup>28</sup> Whether active networks (with myosin motors supplied with ATP) will contract depends on the crosslinker concentration, *e.g.* filamin. A threshold level of crosslinking and inter-connectivity is necessary for geometrically connected network. If the crosslinker concentration is well below that of marginal stability, the network is not connected enough for stresses to propagate, and if the crosslinker concentration is too high, the network may become too stiff to be reorganised.<sup>96</sup>

The crosslinker fimbrin tightly crosslinks actin filaments in parallel bundles and is observed in cellular protrusions such as filopodia and microvilli<sup>97</sup> (see Fig. 7D). The parallel binding greatly increases the bending stiffness, taking them away from the semiflexible regime and allowing them to resist significant compressional forces. The small size of fimbrin prevents myosin from entering the bundles, and consequently, they generate forces solely by polymerisation and growth. Another type of crosslinker is  $\alpha$ -actinin, which, like fimbrin, binds actin filaments together in parallel; but unlike filamin, it is relatively long and leaves more open bundled structures. Their open nature allows non-muscle myosin to interact with antiparallel filaments creating contractile stress fibers (see Fig. 7C). Stress fibers can be long and complex with varied staggering of actin and myosin (as opposed to the regular striated arrangement seen in contractile sarcomeres) but their essential feature of anti-parallel filaments being pulled together by myosin remains the same.<sup>98</sup> Stress fibers in cells adhered to substrate can be classified as ventral or dorsal, where ventral stress fibers develop tension between focal adhesions and its attached substrate, and dorsal stress fibers develop tension between focal adhesions and actin structures deeper in the cell.<sup>98,99</sup>

Branched networks are a key component of the lamellipodia, shown in Fig. 7A, a protruding actin mesh which forms the leading edge of motile cells. Their growth is facilitated by the ARP2/3 complex which nucleates new branches at a 70° angle to existing filaments, and network branches are orientated such that they form a ±35° angle to the leading edge.<sup>100</sup> This orientation is defined by the activation of APR3/2 which is linked to the cell membrane, ensuring network growth and the forces generated are directed towards the membrane. The ARP2/3 crosslink acts as an approximate weld joint, and since the length between filaments is ~100 nm, a ratio of  $L_p/L_c \approx 200$  is

achieved. According to eqn (4), this therefore gives a rest length of  $0.999L_c$ , as such the network filaments are relatively stiff. The suggested high persistence length is confirmed by recent experiments, which demonstrate that the elasticity in branched networks is predominantly enthalpic.<sup>101</sup> The lamellipodia resists compression and its polymerisation generates forces to push the cell's leading edge; a single filament can generate  $\sim 1$  pN as it polymerises.<sup>102</sup> The Euler buckling force of filaments in this network is  $\sim 100$  pN, but as Section 2.1 describes, buckling can occur at lower forces in a thermally fluctuating system. *In vitro* networks formed from reconstituted filaments and APR3/2 complexes give an initial Young's modulus of 1 kPa, much stiffer than typical reconstituted networks which have Young's moduli  $< 100$  Pa owing to their much longer filaments and reduced branching.<sup>71</sup> A schematic of the typical relationship between stress and modulus for branched networks is shown in Fig. 8.

Branched networks have a coordination number of 3, well below the point of marginal stability for central force networks, and owe their stability to the rigid crosslinks and relatively stiff short actin chains between them. Fig. 8 shows the separation of the strain response of such networks into three regimes: linear, stress stiffening, and stress softening. The linear regime arises from the bending elasticity of the network,<sup>103,104</sup> which then enters the stress stiffening regime where the bend-stretch stiffening occurs. In this regime, some chains become aligned to the deformation axis and begin to enthalpically stretch, while others are still subjected to compression. At a critical stress, the compressed chains will begin to buckle, relieving some of the internal stress and the network goes through stress softening with increasing stress. The softening is reversible, as although the chains have buckled, their ends are still attached to the network. Therefore upon the tension being relieved, buckled filaments will return to their unbuckled state.<sup>69</sup> Rheological experiments on branched actin networks reveal power law rheology as described by the GWLC with a low frequency power law exponent of  $\beta = 0.13$ , placing them close to the elastic regime.<sup>69</sup>

Further considerations may be necessary for cytoskeletal networks adsorbed to a membrane, such as those for the

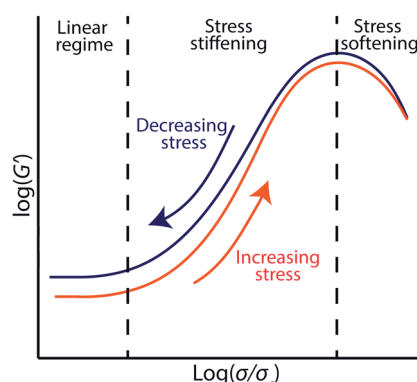


Fig. 8 Schematic of the storage modulus as a function of imposed stress demonstrating the reversible strain stiffening observed in *in vitro* branched actin networks, adapted from ref. 69.

spectrin network in red blood cells (RBCs) where a composite membrane cytoskeletal layer is formed. In this system, somewhat counterintuitively, greater crosslinking to the membrane results in softening, the origin of which lies in the entropic nature of the filaments.<sup>105</sup> Moreover, in such systems the stiffness can be controlled by tuning the active turnover of cross-links and the dissociation rate.<sup>106,107</sup>

## 5 Cell mechanics

The study of cell mechanics is a highly active field, and a plethora of techniques have been developed to probe cells internally, externally, and at varying length scales and frequencies. Fig. 9 shows a schematic of an adhered cell with some of the techniques available for measuring cell rheology. Magnetic twisting cytometry (MTC) uses a magnetic field to oscillate magnetic beads at a set frequency and amplitude. The beads are often coupled directly to the cytoskeleton *via* a fibrin coating which attaches to surface integrins.<sup>59,108</sup> The magnitude of strain is small enough that the cell response is linear, avoiding complicated issues of strain stiffening. Particle tracking microrheology (PTR), including passive, active and two-point rheology, can be used to probe the dynamic modulus of local regions within the cell *via* injected or phagocytosed beads.<sup>27,109</sup> Care should be taken when interpreting the low frequency results of passive microrheology, as the technique is based on the fluctuation-dissipation theorem (FDT) which assumes bead movement originated from thermal motion and the complete averaging over a measurement cycle. However, as cells are active, myosin activity and other active transport may interfere with the passive bead motion. This results in a greater mean squared displacement of a bead measured over longer time scales, falsely inferring a more compliant material.<sup>8,28,33</sup> At high frequencies, FDT is valid again as the biological activity has a time scale approximately  $> 10^{-3}$  s. In comparison to

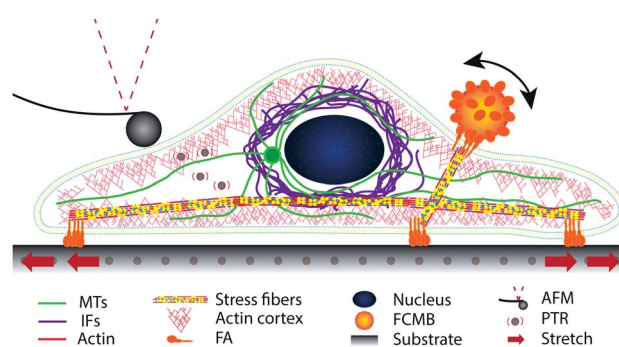


Fig. 9 Scheme of a cell and its cytoskeletal network, and some methods of measuring cell rheology. FA is a focal adhesion and FCMB stands for the fibrin coated magnetic bead which is used in the magnetic cytometry. The fibrin allows the beads to be coupled directly to the cytoskeleton. The beads (single, or multiple) in the cytoskeleton are used for particle tracking rheometry (PTR), which may be active or passive. The AFM cantilever allows high resolution large force measurements to be acquired depending on the attached tip/bead. Another method of applying force to the cell is stretching the substrate beneath it.

passive microrheology, active microrheology, where beads have a driven oscillation *via* magnetic fields of optical tweezers and does not use FDT, is valid for all frequencies.<sup>28,33,109</sup> Atomic force microscopy allows for high resolution large force measurements to be made on cells, but generally accesses lower frequencies of up to 200 Hz.<sup>110,111</sup>

In addition to direct measurement of cellular response to external forces, forces exerted by the cell on their surroundings have also been subjected to intensive studies due to their implications in tissue re-modeling and cell migration. Traction force microscopy can measure the stresses that cells apply to a substrate by tracking the displacement of beads in a substrate of known modulus.<sup>112,113</sup> Recently, this has been extended to cells embedded in 3D substrates to visualise cells in a more physiological environment.<sup>114,115</sup> Global forces can be applied to cells by deforming the substrate, and the response can be measured using either MTC or microrheology for beads embedded in the substrate.<sup>7,116</sup> Other techniques not shown in the figure include: laser cutting, which uses laser nanoscissors to cut cytoskeletal elements and observe relaxation;<sup>112</sup> micro-electromechanical systems (MEMS) for cells, which utilise microfabrication techniques to create a variety of structures to test the mechanical properties;<sup>117</sup> micro/nano fluidics<sup>118</sup> and micromanipulation, in which a force is applied to the cell (*via* a micropipette or micro-pillar) and the transition to a new mechanical equilibrium is monitored (*e.g.* growth of focal adhesions and stress fibers).<sup>119,120</sup>

In this section we look at the mechanical response of the whole cell and its surprisingly consistent behavior, despite the various types of cells and their complexity. We first discuss the different regimes of cell response associated with a rheological measurement, then consider the effects of force-dependent behaviors, and finally give example theoretical models accounting for the observed responses and behaviors.

### 5.1 Power-law cell rheology

Although the reported elastic modulus varies significantly, with values between 0.1 and 10 kPa depending not only on the measurement technique but also on the cell type,<sup>121</sup> the rheology of cells is surprisingly simple. Independent of the technique, the region of the cell, or the cell type, the cell rheology is consistently found to obey a simple power law of the form<sup>7,108,122–125</sup>

$$G^* = A\omega^{\beta_1} + B\omega^{\beta_2}, \quad (11)$$

where  $A$ ,  $B$ ,  $\beta_1$ , and  $\beta_2$  are constants (see Fig. 5). This is often reported as simply  $G^* = A\omega^{\beta_1}$  or an equivalent expression, since the second term  $B\omega^{\beta_2}$  only dominates at high frequencies. This high frequency regime presents itself with a power exponent of  $\beta_2 \approx 3/4$ , alluding to high-frequency single filament response of the cytoskeleton.<sup>124–127</sup> Therefore, our discussion will mainly focus on the  $\beta_1$  power-law, which dominates at the more physiological timescales, or the frequency range  $\sim 0.01$  to 1000 Hz. The rheology here is often described as ‘scale-free’ in reference merely to there being no single characteristic relaxation time.<sup>7,108,123,124</sup> This scale-free rheology and power-law response

was first described by Fabry *et al.*, where it was fitted with a phenomenological model based on soft glass rheology (SGR).<sup>58,59</sup> As discussed in the previous section on GWLC rheology, the exponent  $\beta_1$  describes where the cell (or another network) sits on a scale between completely elastic behaviour (where  $\beta_1 = 0$ ) and purely viscous behaviour (where  $\beta_1 = 1$ ). For any exponent above 0, the cell will never truly see an end to its relaxation and consequently, behaves as a power-law fluid. This is in obvious contradiction to the fact that cells will often exist in a force equilibrium with their environment, and clearly do not relax forever. This may be explained through actin-myosin activity and constant cytoskeletal remodelling, but there is currently no clear answer. Cells typically exhibit  $\beta_1$  values closer to the elastic than the viscous behaviour, in the range of 0.1–0.5. The frequency response of a single cell is not spatially homogeneous, and it has been suggested that there are two regions of distinct rheology. At the actin cortex the power law is lower and the region is more elastic, whereas the deep cell interior has a higher power and is more fluidic.<sup>109,124</sup> In the past, there was some contention as to whether free-floating cells obey this power law, following from experiments carried out with optical tweezers.<sup>128,129</sup> However, these reports have since been amended, and it is believed free-floating cells do obey power law rheology.<sup>130</sup> In addition, one needs to be wary of rheological measurements with large deformations due to the effect of cytosol flow and poroelasticity (discussed below).

The scale-free region holds well in the region of  $\sim 10^{-2}$  to  $10^3$  Hz for small deformations. However, at very low frequencies there have been reports of third, more fluid like, power law, although it is difficult to know if this has meanings in terms of the cytoskeletal structure as extensive remodelling can occur over these time scales.<sup>131,132</sup> Very recently, it has become apparent that the flow of cytosol through the impeding cytoskeletal network will also play a role in cell relaxation.<sup>111</sup> This porous flow relaxation is in addition to the power-law rheology, and is described well in the framework of poroelasticity which gives rise to a single exponential relaxation time determined by the elasticity and pore size of the network, as well as the viscosity of the cytosol. The effects of poroelasticity are only apparent for large deformations and at times less than  $\sim 0.5$  s. Although there are hints of it in previous work,<sup>129,133</sup> it is surprising that this theory has only been reported recently, a fact which the authors attributed to techniques such as MTC and particle tracking rheology being isochoric with little fluid flow.

### 5.2 Effects of prestress

Adhered cells exist in a prestressed state, with tension developed by stress fibers balanced by ECM adhesions and microtubules. The distribution of stress in the cell is non-uniform and is believed to follow discrete cytoskeletal elements.<sup>134,135</sup> The tension can be controlled not only by substrate stiffness but also by cytoskeletal drugs, which moderate cytoskeletal polymerisation and actin-myosin activity. Typically, the stiffer the substrate the greater the tension, but if the substrate is too soft, stress fibers fail to form.<sup>10</sup> In experiments where single stress fibers are cut with laser scissors, it is observed that on soft

substrates a change in cell shape is induced, whereas on stiff substrates many fibers must be cut before a significant change is observed.<sup>112</sup> It is now well established that the cytoskeletal prestress can control the power law exponent value,<sup>8,123,136</sup> as is also true for prestressed actin/filamin-A networks<sup>68,71</sup> described by the GWLC model earlier. The greater the pre-stress, the more elastic the cell becomes, resulting in a higher apparent modulus and a low power-law exponent. Pre-stress may serve many purposes. Firstly, it is obvious that pre-stress can only exist if there is another body imposing an equal and opposite force. For an adhered cell, this is primarily the ECM which allows the cell to mechanically probe the substrate, particularly its stiffness.<sup>137</sup> Another consideration, as discussed in the theoretical section on networks (Section 3.2), is that a 3D network with coordination number of less than 6 is far from stable if only central forces are considered. Although there are different ways to increase stability, pre-stress may be seen as one of the most common origins of network stability and presumably the stability of cytoskeletal networks.

Just like almost all filamentous networks, cells exhibit stress stiffening.<sup>8,122,123</sup> Recently, it has been shown that the extent of stress stiffening strongly relates to the pre-stress, where the greater the internal prestress is, the lower the stress stiffening will be. This is illustrated in Fig. 10 which shows the immediate differential stiffness,  $K'(\sigma)$ , of cells directly after an applied external stress,  $\sigma_e$ , for varying internal prestress,  $\sigma_p$ , as determined from creep experiments on seven cell types.<sup>8</sup> The differential stiffness is defined as  $K' = d\sigma/d\gamma$ , that is, it merely represents the local slope of a non-linear stress-strain relationship. It was observed that as the cell prestress increased, there was a larger initial modulus and a reduced stress stiffening response with respect to the external stress. This was explained with contributions of internal prestress and external prestress following the heuristic relationship  $K'(\sigma) = K'_0 + a(\sigma_p + \sigma_e)$ .<sup>8</sup> This is similar to the approximately linear relationship observed for the actin network formed with filamin.<sup>62</sup>

### 5.3 Fluidisation

Another prominent feature of cell rheology is their ability to fluidise under certain conditions, typically decreasing the shear

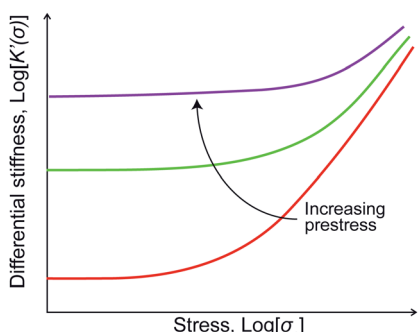


Fig. 10 Shear modulus at zero strain as a function of applied stress for increasing prestress. Adapted from creep experiments by Kollmannsberger *et al.*<sup>8</sup>

modulus and increasing the power exponent. This was first investigated in experiments by Trepaut *et al.*, where the substrate beneath adhered cells was rapidly strained to varying degrees while the dynamic shear modulus was measured using MTC<sup>116</sup> (see Fig. 9). It was found that the larger the stretch, the larger the fluidisation, which means a decreased modulus and an increased power-law exponent. Following fluidisation, cells undergo a period of recovery, where the modulus steadily increased to recover its initial value. Explained in the context of iGWLC, such behaviour can be said to arise from the transient nature of cytoskeletal crosslinks. If a large rapid strain is applied, there is little time for crosslinks to disconnect and reattach; consequently, the large stress build up results in the dissociation of the majority of crosslinks and fluidisation. Following this, there is a period of recovery as the crosslinks reattach and the network reforms.

The creep experiments on cells also exhibit fluidisation behaviour. The creep modulus of a cell is described by  $J(t) = J_0(t/t_0)^{\beta_1}$ , where  $\beta_1$  represents the now familiar power-law fluid rheology of the cell. The fluidisation, defined as an increase in  $\beta_1$ , was observed to be the most pronounced for cells with the greater pre-stress; in contrast, cells with little prestress showed no observable fluidisation. Interestingly and perhaps counter-intuitively, the creep modulus was observed to increase in spite of fluidisation, *i.e.*, the cell becomes more viscous, demonstrating the interplay between stress stiffening and fluidisation. To clarify, equilibrium prestress results in a lower exponent and a greater modulus, but external non-equilibrium stress results in an increased exponent and modulus. Similar responses were

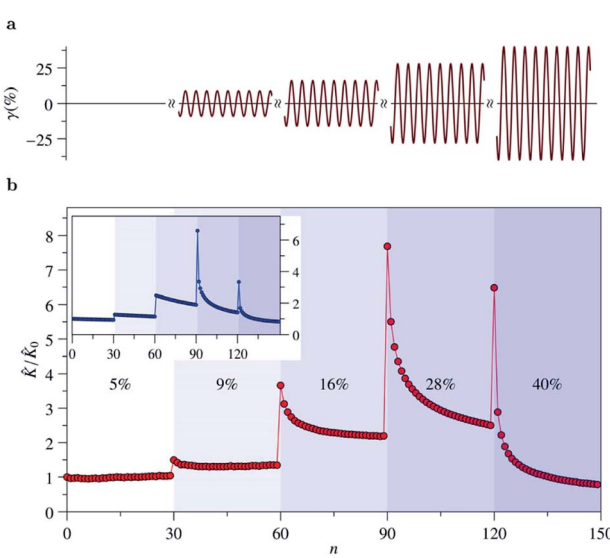


Fig. 11 Inelastic response of F-actin/rigor heavy meromyosin networks relating to the iGWLC model, taken from ref. 56. (a) Shows a schematic of oscillatory shear applied to the network: oscillations are at a constant  $\omega = 0.025$  Hz, and every 30 cycles the strain amplitude is increased. (b) Measured and iGWLC-predicted (inset) differential modulus at peak amplitude as function of the cycle number,  $n$ . Up to 40% strain amplitude, there is a clear increase in modulus and fluidisation (relaxation) with increasing strain amplitude as stress stiffening and fluidisation compete. At 40% strain amplitude, fluidisation dominates and the modulus relaxes quickly to lower than the initial value.

also observed in oscillatory measurements on F-actin/rigor heavy meromyosin networks which are successfully modeled by the iGWLC model (see Fig. 11).<sup>56</sup>

In the context of the iGWLC model, the fluidisation seen in the creep experiments corresponds to the 16% and 28% amplitude response seen in Fig. 11, where the fluidisation occurs but not enough to lower the modulus below that of the zero strain state. In contrast, the larger strains seen in the cell substrate stretching experiments are likely at an amplitude to fluidise the cell to point where the relaxed modulus is lower than that of the zero strain rate, similar to the 40% amplitude oscillations in Fig. 11.

#### 5.4 Theoretical models

After highlighting the key rheological response of a cell in the context of semiflexible networks (*i.e.*, GWLC to iGWLC), it is worth reviewing some other models of cell mechanics. There have been numerous attempts to model and explain the mechanical properties of the cell, but currently no single model explains the full range of mechanical behaviour.<sup>123</sup>

The tensegrity model is a top down approach which models the cell as a prestressed structure of tensed cables and compression resisting elements.<sup>138,139</sup> A tensegrity structure, literally meaning tensional integrity, is typically formed of isolated compression resisting units, connected and stabilised *via* tensional elements (a pertinent example would be a modern dome tent, where tent poles are compressed and the base is under tension). In an adhered cell, it is proposed that tension is generated through stress fibers and actin-myosin machinery, which is balanced by focal adhesions to the ECM and the compression of microtubules. Many facets of cell behaviour agree with tensegrity: prestress increases elasticity;<sup>8,108</sup> forces applied at focal adhesions are transmitted deep into the cell;<sup>140</sup> and microtubules bear compression and buckling increases with prestress.<sup>86,87,140</sup> However, current tensegrity models have not yet accounted for the power-law frequency response<sup>141</sup> or fluidisation, nor do they take into account the entropic nature of its structural elements. This could potentially be resolved by incorporating semiflexible elements, rather than purely enthalpic elements.

The isostatic continuum model proposed by Blumenfeld<sup>142</sup> elegantly demonstrates that it is not necessary to use discrete cytoskeletal models, as is often suggested. In fact, the idea of using discrete models to explain action at a distance is misguided in the assumption that stresses will remain focused over large distances. This is only true for distances on the scale of the mesh size, but in cells, action is observed over distances much larger than the mesh size of cytoskeletal networks.<sup>140</sup> In this case, stresses will disperse and it should be possible to model the behaviour on large scales using classical continuum elasticity theory. However, continuum models can give rise to non-uniform force channeling if their field equations are hyperbolic. Under such differential equations, forces do not spread uniformly but rather follow a characteristic path determined by the equation. Blumenfeld explained that hyperbolic equations could arise if the network is critically isostatic,

meaning that it has only just reached marginal stability.<sup>142</sup> This is not unlikely for cytoskeletal networks, which have coordination numbers far below the critical coordination number of 6 for central force networks (see Section 3.2).

Soft glass rheology (SGR) was first applied by Fabry to explain the rheological properties of cells.<sup>59</sup> The rheological properties of soft glasses, such as foams, emulsions, pastes and slurries, arise from structural disorder and metastability.<sup>58</sup> The mechanics of soft glasses is determined by a distribution of yield energies, or energy traps, which define the metastability of the system, as well as an effective temperature,  $X$ , which determines the ease at which traps are overcome. The resulting dynamics follow a power law of  $\omega^{X-1}$ , where  $X = 1$  is an elastic solid and  $X = 2$  is a viscous fluid.<sup>58</sup> The parallels with cell rheology are compelling, exhibiting low storage and loss moduli (in the range of single Pa to kPa) which increase with frequency as a weak power law,<sup>59,108</sup> fluidisation upon shear,<sup>7,8,116</sup> and anomalous diffusion.<sup>5,108</sup> However, SGR lacks molecular details, and cannot explain strain stiffening or the high-frequency power law. A key postulate of soft glassy rheology is the increase in initial modulus with a decrease in the power-law exponent. This predictable relationship leads to an apparent convergence of extrapolations of cell power laws. This method allows cells to be described by a single parameter, the effective temperature  $X$ , since other constants are identical for all cells.<sup>7,108,109,143</sup> However, the opposite relationship is seen by comparing measurements of single cell type measurements, where a simultaneous increase in modulus and power-law exponent are observed, indicating that stiffer regions have a more fluid like rheology.<sup>108,144</sup> An explanation for this is that, deeper bead indentation and greater attachment to the cytoskeleton mean that features closer to the nuclear envelop were probed, which inevitably resulted in a high modulus and a more viscous response.<sup>108</sup> In all, the above examples illustrate the feasibility of adapting some well-established gel/network theories to explain passive cell behaviors. However, none of the models so far can account for the active contraction of cells.<sup>123</sup>

## 6 Fibrous tissue mechanics

Looking beyond the cytoskeleton, we find that biology is rife with filamentous networks. A common feature of these networks is nonlinear strain stiffening, and it is often alluded that these networks owe their stiffening to semiflexibility. In this section, we explore whether this is the case by looking at prevalent filament forming proteins such as fibrin, collagen, and elastin, as well as the networks they form. Furthermore, we examine how collagen and elastin can work together to tune the elastic properties of soft connective tissues.

#### 6.1 Extracellular matrix fibrils in tissue

**Fibrin.** Fibrin is a filamentous protein formed by fibrinogen and establishes networks that serve as scaffolds for blood clots. The fibers formed have diameters ranging between 10 and 200 nm depending on the formation conditions.<sup>104,145</sup> At a diameter of 10 nm the persistence length is 500 nm, so with typical

network mesh sizes of 270 nm, filaments can be considered to behave semiflexibly.<sup>146</sup> At large diameters the persistence length increases, and filaments become essentially stiff (non-thermal). This leads to transition in the mechanics from entropic elasticity to solely enthalpic elasticity.<sup>104</sup> As discussed in the section on networks (Section 3), nonlinear strain stiffening still occurs in these networks, manifested as the transition from bending elasticity to stretching elasticity: at low strains, the elasticity results from the bending fibers, but at higher deformations fibers align to the strain and begin to stretch, resulting in strain stiffening.<sup>103,104</sup> In general, the mechanical properties of uncrosslinked fibrin networks depend on strain history, a function likely related to adapting to forces at wound sites before becoming crosslinked and exhibiting reversible strain stiffening elasticity.<sup>147</sup>

**Collagen.** Collagen has been expressed since before the cambrian explosion, more than 540 million years ago, and is still produced by all multicellular (metazoan) cells.<sup>3</sup> In mammals, it provides strength, elasticity and structural stability to fibrous tissues. Currently, 28 types of collagen have been identified in the human body, and together they make up one-third of the protein weight.<sup>148</sup> Collagen I, a fibril-forming collagen, accounts for around 90% of collagen and is the main structural component of connective tissues such as tendons, fascia, and bone.<sup>149</sup> It is heavily researched and often used to create reconstituted collagen gels;<sup>150</sup> accordingly, collagen I will be referred to as plain collagen from now on.

Whether collagen fibrils are semiflexible can be difficult to ascertain, primarily as a consequence of the hierarchical structures of collagen. A single collagen molecule is formed by left-handed alpha peptide strands, which come together to form a right handed triple helix of contour length  $\approx 300$  nm and diameter of 1.5 nm stabilised by numerous hydrogen bonds. A range of values have been reported for the single molecule persistence length, including 175 nm (calculated from hydrodynamics),<sup>151</sup> 95 nm (calculated from sedimentation constants and intrinsic viscosity),<sup>152</sup> 57 nm (measured from electron micrographs),<sup>153</sup> and 14.5 nm (the WLC model fitted to a single molecule for extension).<sup>154</sup> A recent article reports that differences can be explained by the technique and the environment collagen that has been tested in ref. 155. There are also measurements of the persistence length of collagen molecules in varying solutions by analysis of molecular conformations on a 2D surface as characterised by AFM. It was found that in deionized water, collagen is relatively flexible with a persistence length of 12 nm, whereas in fetal bovine serum (FBS) and phosphate buffer solution (PBS), the persistence lengths were 135 nm and 162 nm, respectively. Regardless of the explicit value, the persistence lengths of single collagen molecules are clearly in the range of semiflexibility.

*In vivo* and *in vitro* (under suitable conditions), molecules of collagen will aggregate through entropic and electrostatic interactions to form collagen fibrils with a distribution of diameters (100–500 nm). The fibril structure is highly ordered, with molecules aligned parallel to the fibril axis and staggered with respect to their neighbours. The staggering of molecules creates regular overlap regions of length 31 nm and gap regions

of length 36 nm, both repeat every 67 nm and are visible as the well known D-banding seen in electron micrographs (see Fig. 14F). Crosslinking can further stabilise the fibril: with low crosslinking fibrils being more dissipative and show large yield regimes, but with increasing crosslinks fibrils become stiffer and more brittle.<sup>156</sup> A common approach for calculating the bending stiffness of a filament is to use the relation  $A = YI$ , where  $Y$  is the Young's modulus and  $I$  is the second moment of area equivalent to  $\pi r^4/2$  for a rod.<sup>21</sup> However, this relation is based on elastic continuum theory and is only valid for isotropic homogeneous materials. As collagen fibrils are structurally anisotropic and there may be internal shear, it is important to test the bending modulus directly. This has been done by Yang *et al.* who bent collagen fibrils at different length scales using AFM under physiological conditions.<sup>157</sup> From their results, the lowest bending stiffness was  $6.4 \times 10^{-19}$  N m<sup>2</sup> corresponding to a persistence length of  $\sim 10$  m. From further comparison to the Young's modulus of other experiments, which are typically between 0.3 and 2 GPa, and assuming the relation  $A = YI$  is approximately valid, it can be inferred that the persistence length is just under 1 mm when the diameter is less than 20 nm. Consequently, collagen fibrils are unlikely to be semiflexible under most conditions, and as other reports suggest, they are better described by athermal models of nonaffine stretching.<sup>49,158,159</sup> Experimental evidence supports this, with analysis of scanning confocal microscopy images of collagen networks reporting that the persistence length of *in vitro* networks is greater than 1 cm.<sup>160</sup> This may not be true for reconstituted fibrils of a particularly low modulus or diameter; but in the biological settings, collagen fibrils are rarely less than 100 nm.<sup>161</sup>

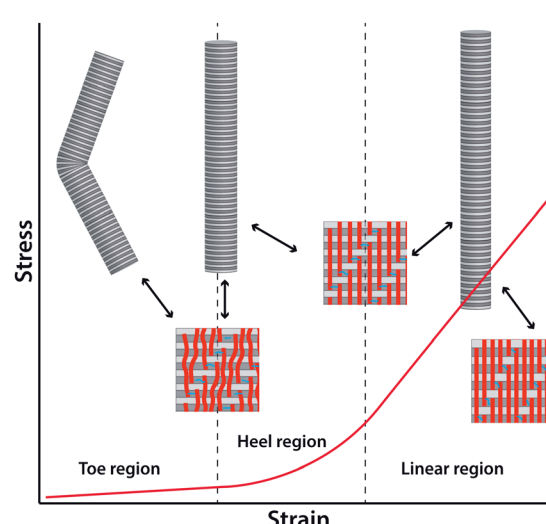


**Fig. 12** Collagen fibril response to strain. Toe region: the initially wavy (crimped) fiber is straightened, accompanied by a small linear in stress. Heel region: once the fiber is straight, strain causes the straightening and alignment of individual collagen molecules in the fiber, and there is an internal entropic origin to the elasticity. There is lengthening of the fiber but little change to the D-banding separation. The linear region: once the collagen molecules have been aligned, strain induces the interfibrillar sliding of collagen molecules and the stretching of crosslinks.<sup>163–166</sup> Beyond this, there will be the breaking of crosslinks and fiber failure.

Although collagen fibrils are generally not semiflexible, they do exhibit nonlinear strain dependence due to their internal structure. Fig. 12 illustrates the strain stiffening behaviour of a single collagen fibril in solution. The strain response is separated into three regions: the toe, the heel, and the linear region. The toe region is simply a consequence of the natural waviness, sometimes called crimp, of the fiber being removed resulting in a linear, low modulus region from fiber bending. The constituent collagen molecules are not perfectly aligned to the fibril axis and whilst in solution they fluctuate. Once the fibril is straight, the molecules begin to straighten and the fluctuations are pulled out, resulting in the observed strain stiffening heel region. The heel region does not exist in dry fibrils tested *in vitro* as molecules are closely packed with no solution providing electrostatic shielding; consequently, dry fibrils behave linearly once straightened.<sup>162,163</sup> Following the heel region and the straightening of molecules in wet fibrils, a liner regime is entered where elasticity results from the interfibrillar sliding of collagen molecules and the stretching of crosslinks.<sup>163–167</sup>

**Elastin.** Elastin fibers comprise an outer core of microfibrillar mantle and an inner core of amorphous crosslinked elastin.<sup>168</sup> The fibers provide elastic recoil and elasticity to fibrous tissues. They are the most resilient proteins in the body, typically lasting a life time, having a half-life of 74 years.<sup>169</sup> The microfibrillar sheath is constructed mainly of fibrillins and is believed to act as a scaffold during elastin deposition and is essential for fiber integrity.<sup>168</sup> The elastin core is formed by crosslinked tropoelastin, which has only recently had its nanostructure resolved,<sup>170</sup> and is an asymmetric molecule with two functionally distinct regions separated by a long elastic coil region.<sup>170–172</sup> The elasticity of single tropoelastin is well defined by the WLC model, with a persistence length of  $\sim 0.35$  nm and a contour length of  $\sim 166$  nm.<sup>170</sup> However, as  $L_p/L_c$  is rather small, and the resting length is  $\sim 20$  nm, the stress-strain curve is only nonlinear at high strains. Tropoelastin is highly elastic, withstanding up to 800% strain with no observable hysteresis. Upon crosslinking, the extensibility is reduced and elasticity is increased.<sup>173</sup> Single elastin fibers *in vivo*, constructed from crosslinked tropoelastin in a microfibril shell, are extensible up to  $\sim 200\%$  and have a linear response up to  $\sim 100\%$  strain with a Young's modulus ranging between 0.1 and 1.2 MPa, but on average 0.4 MPa.<sup>2,174</sup>

## 6.2 Soft connective tissue

Soft connective tissue consists of an extracellular matrix and denizen cells, the most prevalent of which are fibroblasts (or the close variants, such as tenocytes and myofibroblasts); examples of connective tissue are fascia, ligaments and tendons. The primary constituents of ECM are glycosaminoglycans (GAGs), proteoglycans (PGs), collagen fibers, and elastin fibers. GAGs are linear unbranched polymers of repeating disaccharides composed of a hexosamine and a uronic acid, the most common GAG being hyaluronan; they are highly negatively charged and osmotically active, drawing water into the interstitial spaces.<sup>175</sup> GAGs occupy much of the space of the ECM and form hydrogels at low concentrations, their high osmotic

activity drives the influx of water keeping the ECM turgid and providing mechanical strength against compression. All GAGs apart from hyaluronan will covalently bind to a protein forming proteoglycans. Collagen and elastin fibers act to reinforce the ECM providing mechanical strength and elasticity, the properties of which depend on their concentration and organisation (see Fig. 13).

The common aspect of all fibrous tissues is their nonlinear strain response, observed as an initial linear response with small modulus which remains up to a characteristic strain. Beyond this strain, the modulus increases smoothly and substantially until a second linear regime is reached (similar to the response in Fig. 12 and 2).<sup>176–180</sup> This transition between regimes has many names, including the heel region, transition region, and recruitment region. The exact mechanical behaviour will depend on the organisation of collagen and elastin as well their quantities, leading to a high level of tunability.

Fig. 13B shows a schematic of elastin and collagen networks in subcutaneous fascia (or loose areolar tissue). Collagen fibers take meandering paths, forming a loose network of randomly oriented fibers, and at low strains, collagen fibers offer little resistance (see Fig. 12). Consequently, the elastin network is important for small strain elasticity, and is believed to be important for recoil post-strain, which assists collagen fibers in returning quickly to their rest position.<sup>181</sup> Elastin networks are also suggested to play a similar role in ligaments.<sup>182</sup> At larger strains, the response is dominated by the collagen response, and the connective tissue quickly stiffens with an order of magnitude increase in the differential modulus.<sup>183</sup> The interplay between collagen and elastin fibers is particularly important in tissues such as the lung<sup>184</sup> and the cardiovascular system,<sup>2</sup> where elastin allows large elastic deformations with low

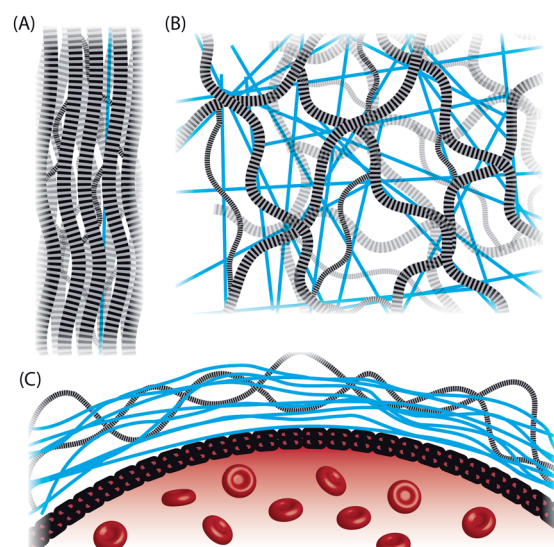


Fig. 13 Types of connective tissue structure: (A) tendon formed by bundled fibers arranged in parallel to the typical stress, there are a few elastin fibers. (B) Subcutaneous tissue with wavy randomly oriented collagen fibers with an underlying elastin network. (C) Inner elastic layer of an artery, formed by a few wavy collagen fibers and dense elastin fiber network.

hysteresis, and wavy collagen fibers protect the tissue from damage at large distensions. Fig. 13C shows a schematic of the inner layer of an artery, where blood pressure is maintained to a high tolerance between heart-beats due their elasticity. The outer collagen sheath limits distension, helping the artery maintain integrity.<sup>2</sup> This can be seen in Fig. 14A and B, which shows the collagen network in an artery at zero pressure and at 140 mmHg taken with a 3D fluorescence laser confocal microscope.<sup>185</sup> Indeed, mice without this collagen sheath die suddenly in late development caused by aortic rupture.<sup>186</sup>

Tendons transmit force between muscle and bone and must withstand large stresses. Tendons contain little elastin (~2% the dry weight compared to collagens at 60–85%)<sup>189</sup> and the mechanical properties are primarily down to the organisation of collagen, which is highly aligned to the predominant strain direction (see Fig. 13A). The constituent fibrils vary in diameter, where it is thought that small diameter fibrils act more elastically, whereas larger fibrils can withstand larger stresses (a perpendicular cross-section can be seen in Fig. 14E).<sup>187</sup> Fibrils are connected laterally to each other and bundled together *via* non-covalently bonded proteoglycan bridges, which occur

periodically every 64–68 nm (comparable to the D-period). Once fibers are formed, their removal does little to change the fibril arrangement.<sup>190</sup> Although they are non-covalently linked, their binding strength exceeds the failure strength of the GAG chain, which has a maximum chain stiffness of  $3.1 \times 10^{-11}$  N nm<sup>-1</sup>.<sup>191</sup> There is experimental evidence that collagen fibrils in ligaments and tendons are long (on the mm scale), and either span the length of the tissue or are long enough to be considered functionally continuous.<sup>161</sup> Whether or not this is true has led to some controversy over the significance of proteoglycan bridges to tendon mechanical properties, and to whether proteoglycan bridges may be important in transmitting stresses between collagen fibrils. However, experiments have shown that partial enzymatic depletion of GAGs does little to alter the modulus at physiological strains.<sup>192</sup> Indeed, their role is little needed if collagen fibers are functionally continuous, such that collagen fibrils split and join into other fibrils, as has been observed.<sup>161,187</sup> This is reinforced by tendon models which show that for long collagen fibrils, proteoglycan depletion will have little effect on the mechanical properties; however, if fibrils are short enough, proteoglycan depletion reduces the mechanical strength considerably.<sup>193</sup>

In excised tendons, collagen fibers are highly crimped (see Fig. 14C), but also overlap and cross-over each other.<sup>194</sup> Upon stretching, their straightening is clearly visible and associated with the heel region<sup>195</sup> (see Fig. 14D). This realignment and straightening of crimped (wavy) collagen fibers in tendons has been confirmed in experiments of fiber visualisation using multiphoton microscopy<sup>180</sup> and changes in the tissue's light polarisability.<sup>177,178,188</sup> The strain stiffening response of tendons is primarily believed to be a result of individual fiber recruitment;<sup>196</sup> although, as we have seen there are many other contributors to nonlinearity, such as the individual collagen fibril response. This follows from individual fibers being crimped to varying degrees, as the tendon is stretched individual fibers will begin to be recruited, steadily increasing the modulus. At a critical strain, all fibers will have straightened and the response will be approximately linear. This is corroborated by experiments, where shortly after crimp is extinguished (typically 2–3% strain), the tendon response is linear and elasticity results from interfibrillar sliding facilitated by the stretching of crosslinks.<sup>164–166,196</sup> *In vivo*, tendons are always under some tension, and it is believed they operate somewhere in the onset of the strain stiffening region.<sup>197</sup>

### 6.3 Theoretical models

Most models focus on the unwinding of fiber crimp rather than the nonlinear response of individual fibrils, all of which follow from collagen fibers in tissue effectively being the only tension bearing elements.<sup>179,198,199</sup> The ideas follow from early work on solids reinforced by inextensible rods,<sup>200</sup> and have since been modified by many others to account for extensibility and waviness.<sup>201</sup> A more recent model which relates measurable quantities to nonlinear strain stiffening is proposed by Cacho *et al.*, in which the distribution of collagen fiber crimp is used to determine when the toe region occurs and what happens

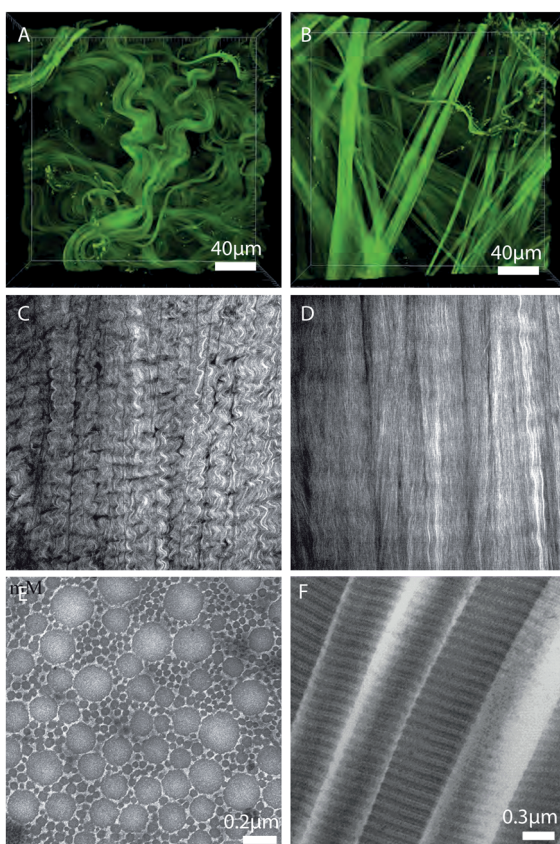


Fig. 14 Collagen fibers in (A) unstrained aorta and (B) strained aorta, acquired by staining collagen with CNA35 and using 3D laser confocal microscopy. Adapted from ref. 185. Collagen fibers in (C) unstrained tendon and (D) strained tendon acquired using multiphoton microscopy. Adapted from ref. 180. (E) Transverse TEM image showing the arrangement and varied diameter of collagen fibrils in the tendon. Adapted from ref. 187. (F) High magnification of collagen fibrils showing the characteristic 67 nm D-banding. Adapted from ref. 188.

Published on 08 January 2014. Downloaded by Michigan State University on 25/01/2016 15:59:36.

afterwards.<sup>179</sup> The tissue in question can be defined by a statistical distribution of fiber waviness, which is expected to follow a Beta distribution defined by two parameters. This distribution has indeed been observed and measured experimentally in the adventitia of rabbit common carotid arteries using computer analysis of 3D laser scanning fluorescence confocal microscopy.<sup>202</sup> As the tissue is stretched, fibers will straighten and eventually contribute to tension by stretching. A simple case is where all fibers are aligned to the stretch axis, where the combined tissue energy for uniaxial strain  $\lambda$  is given by a convolution across different regions in the composite material:

$$F_{\text{tissue}} = F_{\text{matrix}}(\lambda) + \int_0^{\lambda} F_{\text{fiber}}(\bar{\lambda} - l) p_l^m(\mu, \gamma; \bar{\lambda}) d\bar{\lambda}. \quad (12)$$

The  $F_{\text{matrix}}(\lambda)$  term describes the continuum elasticity of the underlying matrix; this will include parts of the ECM that contribute linearly to all uniaxial strain,  $\lambda$ , such as the elastin fiber network and GAG hydrogel. The integral defines the contribution of collagen fibers, where  $p_l^m(\mu, \gamma; \bar{\lambda})$  is the energy contribution of a single fiber at strain  $\bar{\lambda}$ .  $l$  defines the strain at which fibers will first be straight and contributing to strain energy. The  $p_l^m(\mu, \gamma; \bar{\lambda})$  term is the probability distribution which defines how many fibers will contribute to the strain energy at  $\bar{\lambda}$ ; it is parameterised by the constants  $\mu$  and  $\gamma$ , which can be determined from experiments. The indices  $l$  and  $m$  define the lower and upper limits at which fibers may contribute to the strain, respectively, and ensures the integral is zero outside these limits. In essence, the probability distribution defines the recruitment of fibers. If the strain goes beyond a critical stretch, fibers will begin to fail and the elasticity will no longer be reversible. Depending on the crimp distribution, more complicated situations may occur in which fibers begin to break before other fibers have been recruited. Many more advanced models based on these schemes exist, where fiber orientation and bending may be considered, see ref. 179 and 203 for details.

## 7 Conclusions

This brief review tried to summarise a vast and rapidly increasing amount of research on equilibrium and dynamic mechanical characteristics of living systems: metazoan cells and tissues. Naturally, since the mechanics of these systems is essentially controlled by delicately and hierarchically structured filaments, we first revise the present physical knowledge of such filaments. At two extremes, very flexible, entropic chains and very rigid athermal rods, the properties of such filaments are well understood, in polymer physics and elasticity theory, respectively. In between these limits lies an interesting region of semiflexible chains where the characteristic energy thermal motion is comparable in magnitude with the overall elastic energy of filament deformation (mostly bending, but occasionally stretching as well). Physics of semiflexible filaments has recently reached a point of completion, both in their equilibrium and dynamic properties, and we tried to bring the latest

and most accurate results to this review – by necessity having to overlook a large and often famous history of development.

Networks of semiflexible filaments are at the core of mechanical properties of cells, but it is too early to say that the physics of such networks is well understood. The reason is that there is a large variety of possible ways to crosslink such a network; we review the types of crosslinks relevant in the biological context, and the physical consequences on the continuum mechanics of the network. We actually discuss the types of crosslinks in greater detail in Section 4, in the specific context of cytoskeleton, so the reader should remain patient in the more generic ‘networks’ section. In the mechanics of filamentous networks the main issues are the marginal stability at low crosslink functionality, the non-affinity of local deformations that leads to significant softening of networks with low connectivity, the non-linear stress-stiffening of more densely crosslinked filamentous networks – and of course the frequency-dependent response leading to the high-frequency stiffening in certain regimes, and conversely, to high-frequency fluidisation in other regimes and structures (both relevant and frequently utilised in cells).

Actin, intermediate and microtubular filaments are each playing a role in the resulting mechanics of the cell and cell collectives. Here we had to stay away from another very exciting and rapidly developing field of active systems, where the mechanical properties are determined by the (inherently non-equilibrium) motor-driven molecular elements. The only instance when the active motion was relevant in this review was in the context of pre-stress generated and having a profound effect on the resulting response in cells. In contrast, the mechanics of essentially extracellular connective tissue is controlled by the structure of larger-scale filaments (mostly, although not uniquely, made of collagen) and their arrangement in the matrix of other extra-cellular polymers. In this area the experiments and theoretical modelling are still far from achieving a good match, although there are many fundamental properties of connective tissue, relevant for its biological function, that are understood better by virtue of their direct link with the basic filamentous network mechanics. We hope that an extensive list of current original literature will help the readers to orient in this maze of information and find the required threads.

## Acknowledgements

This work was supported by EPSRC UK (RHP), the Ernest Oppenheimer Fund and the Engineering Department starting fund, Cambridge (YYSH). We have benefited from many useful discussions with J.R. Blundell, R.B. Blumenfeld and A. Zaccione.

## References

- 1 B. Wickstead and K. Gull, *J. Cell Biol.*, 2011, **194**, 513–525.
- 2 G. Faury, *Pathol. Biol.*, 2001, **49**, 310–325.
- 3 S. Özbek, P. G. Balasubramanian, R. Chiquet-Ehrismann, R. P. Tucker and J. C. Adams, *Mol. Biol. Cell*, 2010, **21**, 4300–4305.
- 4 R. O. Hynes, *J. Cell Biol.*, 2012, **196**, 671–679.

- 5 P. Bursac, G. Lenormand, B. Fabry, M. Oliver, D. A. Weitz, V. Viasnoff, J. P. Butler and J. J. Fredberg, *Nat. Mater.*, 2005, **4**, 557–561.
- 6 D. A. Fletcher and R. D. Mullins, *Nature*, 2010, **463**, 485–492.
- 7 X. Trepaut, G. Lenormand and J. J. Fredberg, *Soft Matter*, 2008, **4**, 1750–1759.
- 8 P. Kollmannsberger, C. T. Mierke and B. Fabry, *Soft Matter*, 2011, **7**, 3127–3132.
- 9 P. Friedl, K. Wolf and J. Lammerding, *Curr. Opin. Cell Biol.*, 2011, **23**, 55–64.
- 10 T. Lecuit, P.-F. Lenne and E. Munro, *Annu. Rev. Cell Dev. Biol.*, 2011, **27**, 157–184.
- 11 N. Wang, I. M. Tolić-Nørrelykke, J. Chen, S. M. Mijailovich, J. P. Butler, J. J. Fredberg and D. Stamenović, *Am. J. Physiol.: Cell Physiol.*, 2002, **282**, C606–C616.
- 12 C. S. Chen, M. Mrksich, S. Huang, G. M. Whitesides and D. E. Ingber, *Science*, 1997, **276**, 1425–1428.
- 13 A. J. Engler, S. Sen, H. L. Sweeney and D. E. Discher, *Cell*, 2006, **126**, 677–689.
- 14 H. Daniels, *Proc. - R. Soc. Edinburgh, Sect. A: Math.*, 1952, **63**, 290–311.
- 15 J. Hermans and R. Ullman, *Physica*, 1952, **18**, 951–971.
- 16 J. Wilhelm and E. Frey, *Phys. Rev. Lett.*, 1996, **77**, 2581.
- 17 B. Hamprecht and H. Kleinert, *Phys. Rev. E: Stat., Nonlinear, Soft Matter Phys.*, 2005, **71**, 031803.
- 18 B. Hu, V. Shenoy and Y. Lin, *J. Mech. Phys. Solids*, 2012, **60**, 1941–1951.
- 19 J. R. Blundell and E. M. Terentjev, *Macromolecules*, 2009, **42**, 5388–5394.
- 20 J. H. Hartwig and P. Shevlin, *J. Cell Biol.*, 1986, **103**, 1007–1020.
- 21 L. Landau and E. Lifshitz, *The theory of elasticity*, Pergamon, Oxford, 1986.
- 22 G. A. Holzapfel and R. W. Ogden, *Acta Biomater.*, 2013, **9**, 7320–7325.
- 23 J. Blundell and E. Terentjev, *Soft Matter*, 2009, **5**, 4015–4020.
- 24 O. Hallatschek, E. Frey and K. Kroy, *Phys. Rev. E: Stat., Nonlinear, Soft Matter Phys.*, 2007, **75**, 031905.
- 25 K. Kroy and J. Glaser, *New. J. Phys.*, 2007, **9**, 416.
- 26 C. Semmrich, T. Storz, J. Glaser, R. Merkel, A. R. Bausch and K. Kroy, *Proc. Natl. Acad. Sci. U. S. A.*, 2007, **104**, 20199–20203.
- 27 T. M. Squires and T. G. Mason, *Annu. Rev. Fluid Mech.*, 2009, **42**, 413.
- 28 D. Mizuno, D. Head, F. MacKintosh and C. Schmidt, *Macromolecules*, 2008, **41**, 7194–7202.
- 29 F. Gittes and F. MacKintosh, *Phys. Rev. E: Stat. Phys., Plasmas, Fluids, Relat. Interdiscip. Top.*, 1998, **58**, R1241.
- 30 G. Koenderink, M. Atakhorrami, F. MacKintosh and C. Schmidt, *Phys. Rev. Lett.*, 2006, **96**, 138307.
- 31 D. C. Morse, *Macromolecules*, 1998, **31**, 7030–7043.
- 32 F. Gittes, B. Schnurr, P. Olmsted, F. MacKintosh and C. Schmidt, *Phys. Rev. Lett.*, 1997, **79**, 3286.
- 33 D. Mizuno, C. Tardin, C. Schmidt and F. MacKintosh, *Science*, 2007, **315**, 370–373.
- 34 A. Caspi, M. Elbaum, R. Granek, A. Lachish and D. Zbaida, *Phys. Rev. Lett.*, 1998, **80**, 1106.
- 35 R. C. Picu, *Soft Matter*, 2011, **7**, 6768–6785.
- 36 C. Heussing, *New. J. Phys.*, 2012, **14**, 095029.
- 37 C. Broedersz, C. Storm and F. MacKintosh, *Phys. Rev. Lett.*, 2008, **101**, 118103.
- 38 K. Kasza, G. Koenderink, Y. Lin, C. Broedersz, W. Messner, F. Nakamura, T. Stossel, F. MacKintosh and D. Weitz, *Phys. Rev. E: Stat., Nonlinear, Soft Matter Phys.*, 2009, **79**, 041928.
- 39 A. Zoccone, J. R. Blundell and E. M. Terentjev, *Phys. Rev. B: Condens. Matter Mater. Phys.*, 2011, **84**, 174119.
- 40 M. Das, D. Quint and J. Schwarz, *PLoS One*, 2012, **7**, e35939.
- 41 J. C. Maxwell, *Philos. Mag.*, 1864, **27**, 294–299.
- 42 C. J. Derham and A. G. Thomas, *Rubber Chem. Technol.*, 1977, **50**, 830.
- 43 T. J. Pond, *J. Nat. Rubber Res.*, 1989, **4**, 93.
- 44 C. Broedersz, M. Sheinman and F. MacKintosh, *Phys. Rev. Lett.*, 2012, **108**, 078102.
- 45 C. P. Broedersz, X. Mao, T. C. Lubensky and F. C. MacKintosh, *Nat. Phys.*, 2011, **7**, 983–988.
- 46 J. R. Blundell and E. M. Terentjev, *Proc. R. Soc. A*, 2011, **467**, 2330–2349.
- 47 B. DiDonna and T. Lubensky, *Phys. Rev. E: Stat., Nonlinear, Soft Matter Phys.*, 2005, **72**, 066619.
- 48 D. Head, A. Levine and F. MacKintosh, *Phys. Rev. E: Stat., Nonlinear, Soft Matter Phys.*, 2003, **68**, 061907.
- 49 C. Heussinger and E. Frey, *Phys. Rev. E: Stat., Nonlinear, Soft Matter Phys.*, 2007, **75**, 011917.
- 50 M. Gardel, J. Shin, F. MacKintosh, L. Mahadevan, P. Matsudaira and D. Weitz, *Science*, 2004, **304**, 1301–1305.
- 51 B. Wagner, R. Tharmann, I. Haase, M. Fischer and A. Bausch, *Proc. Natl. Acad. Sci. U. S. A.*, 2006, **103**, 13974–13978.
- 52 M. Warner and E. M. Terentjev, *Liquid crystal elastomers*, Oxford University Press, 2003, vol. 120.
- 53 F. MacKintosh, J. Käs and P. Janmey, *Phys. Rev. Lett.*, 1995, **75**, 4425.
- 54 K. Kroy, *Soft Matter*, 2008, **4**, 2323–2330.
- 55 L. Wolff, P. Fernandez and K. Kroy, *New. J. Phys.*, 2010, **12**, 053024.
- 56 L. Wolff, P. Fernández and K. Kroy, *PLoS One*, 2012, **7**, e40063.
- 57 L. Wolff and K. Kroy, *Phys. Rev. E: Stat., Nonlinear, Soft Matter Phys.*, 2012, **86**, 040901.
- 58 P. Sollich, F. Lequeux, P. Hébraud and M. E. Cates, *Phys. Rev. Lett.*, 1997, **78**, 2020.
- 59 B. Fabry, G. N. Maksym, J. P. Butler, M. Glogauer, D. Navajas and J. J. Fredberg, *Phys. Rev. Lett.*, 2001, **87**, 148102.
- 60 A. Palmer, J. Xu and D. Wirtz, *Rheol. Acta*, 1998, **37**, 97–106.
- 61 R. Tharmann, M. Claessens and A. Bausch, *Phys. Rev. Lett.*, 2007, **98**, 088103.
- 62 M. Gardel, F. Nakamura, J. Hartwig, J. C. Crocker, T. Stossel and D. Weitz, *Phys. Rev. Lett.*, 2006, **96**, 088102.
- 63 T. Bretschneider, K. Anderson, M. Ecke, A. Müller-Taubenberger, B. Schröth-Diez, H. C. Ishikawa-Ankerhold and G. Gerisch, *Biophys. J.*, 2009, **96**, 2888–2900.
- 64 K. F. Swaney, C.-H. Huang and P. N. Devreotes, *Annu. Rev. Biophys.*, 2010, **39**, 265–289.

- 65 N. Koder, D. Yamamoto, R. Ishikawa and T. Ando, *Nature*, 2010, **468**, 72–76.
- 66 F. Backouche, L. Haviv, D. Groswasser and A. Bernheim-Groswasser, *Phys. Biol.*, 2006, **3**, 264.
- 67 K. Kasza, F. Nakamura, S. Hu, P. Kollmannsberger, N. Bonakdar, B. Fabry, T. Stossel, N. Wang and D. Weitz, *Biophys. J.*, 2009, **96**, 4326–4335.
- 68 G. H. Koenderink, Z. Dogic, F. Nakamura, P. M. Bendix, F. C. MacKintosh, J. H. Hartwig, T. P. Stossel and D. A. Weitz, *Proc. Natl. Acad. Sci. U. S. A.*, 2009, **106**, 15192–15197.
- 69 O. Chaudhuri, S. H. Parekh and D. A. Fletcher, *Nature*, 2007, **445**, 295–298.
- 70 B. Bugyi and M.-F. Carlier, *Annu. Rev. Biophys.*, 2010, **39**, 449–470.
- 71 M. Gardel, F. Nakamura, J. Hartwig, J. Crocker, T. Stossel and D. Weitz, *Proc. Natl. Acad. Sci. U. S. A.*, 2006, **103**, 1762–1767.
- 72 A.-C. Reymann, R. Boujemaa-Paterski, J.-L. Martiel, C. Guérin, W. Cao, H. F. Chin, M. Enrique, M. Théry and L. Blanchoin, *Science*, 2012, **336**, 1310–1314.
- 73 A.-C. Reymann, J.-L. Martiel, T. Cambier, L. Blanchoin, R. Boujemaa-Paterski and M. Théry, *Nat. Mater.*, 2010, **9**, 827–832.
- 74 L.-L. Pontani, J. Van der Gucht, G. Salbreux, J. Heuvingh, J.-F. Joanny and C. Sykes, *Biophys. J.*, 2009, **96**, 192–198.
- 75 R. Windoffer, M. Beil, T. M. Magin and R. E. Leube, *J. Cell Biol.*, 2011, **194**, 669–678.
- 76 H. Herrmann, S. V. Strelkov, P. Burkhard and U. Aebi, *J. Clin. Invest.*, 2009, **119**, 1772.
- 77 K. H. Yoon, M. Yoon, R. D. Moir, S. Khuon, F. W. Flitney and R. D. Goldman, *J. Cell Biol.*, 2001, **153**, 503–516.
- 78 M. Plodinec, M. Loparic, R. Suettlerlin, H. Herrmann, U. Aebi and C.-A. Schoenenberger, *J. Struct. Biol.*, 2011, **174**, 476–484.
- 79 N. Wang and D. Stamenović, *Am. J. Physiol.: Cell Physiol.*, 2000, **279**, C188–C194.
- 80 F. Pampaloni, G. Lattanzi, A. Jonáš, T. Surrey, E. Frey and E.-L. Florin, *Proc. Natl. Acad. Sci. U. S. A.*, 2006, **103**, 10248–10253.
- 81 E.-M. Mandelkow, E. Mandelkow and R. A. Milligan, *J. Cell Biol.*, 1991, **114**, 977–991.
- 82 A. Caspi, R. Granek and M. Elbaum, *Phys. Rev. E: Stat., Nonlinear, Soft Matter Phys.*, 2002, **66**, 011916.
- 83 V. Pelletier, N. Gal, P. Fournier and M. L. Kilfoil, *Phys. Rev. Lett.*, 2009, **102**, 188303.
- 84 M. Das and F. MacKintosh, *Phys. Rev. E: Stat., Nonlinear, Soft Matter Phys.*, 2011, **84**, 061906.
- 85 Y.-C. Lin, G. H. Koenderink, F. C. MacKintosh and D. A. Weitz, *Soft Matter*, 2011, **7**, 902–906.
- 86 D. Stamenović, S. M. Mijailovich, I. M. Tolić-Nørrelykke, J. Chen and N. Wang, *Am. J. Physiol.: Cell Physiol.*, 2002, **282**, C617–C624.
- 87 C. P. Brangwynne, F. C. MacKintosh, S. Kumar, N. A. Geisse, J. Talbot, L. Mahadevan, K. K. Parker, D. E. Ingber and D. A. Weitz, *J. Cell Biol.*, 2006, **173**, 733–741.
- 88 M. Mehrbod and M. R. Mofrad, *PLoS One*, 2011, **6**, e25627.
- 89 B. Geiger, J. P. Spatz and A. D. Bershadsky, *Nat. Rev. Mol. Cell Biol.*, 2009, **10**, 21–33.
- 90 G. Jiang, G. Giannone, D. R. Critchley, E. Fukumoto and M. P. Sheetz, *Nature*, 2003, **424**, 334–337.
- 91 C. G. Galbraith, K. M. Yamada and M. P. Sheetz, *J. Cell Biol.*, 2002, **159**, 695–705.
- 92 W. Goldmann and G. Isenberg, *FEBS Lett.*, 1993, **336**, 408–410.
- 93 O. Lieleg, M. M. Claessens and A. R. Bausch, *Soft Matter*, 2010, **6**, 218–225.
- 94 K. Schmoller, O. Lieleg and A. Bausch, *Biophys. J.*, 2009, **97**, 83–89.
- 95 K. M. Schmoller, O. Lieleg and A. R. Bausch, *Soft Matter*, 2008, **4**, 2365–2367.
- 96 P. M. Bendix, G. H. Koenderink, D. Cuvelier, Z. Dogic, B. N. Koeleman, W. M. Brieher, C. M. Field, L. Mahadevan and D. A. Weitz, *Biophys. J.*, 2008, **94**, 3126–3136.
- 97 A. Bretscher, *Proc. Natl. Acad. Sci. U. S. A.*, 1981, **78**, 6849–6853.
- 98 S. Pellegrin and H. Mellor, *J. Cell Sci.*, 2007, **120**, 3491–3499.
- 99 U. S. Schwarz and M. L. Gardel, *J. Cell Sci.*, 2012, **125**, 3051–3060.
- 100 T. M. Svitkina and G. G. Borisy, *J. Cell Biol.*, 1999, **145**, 1009–1026.
- 101 T. Pujol, O. du Roure, M. Fermigier and J. Heuvingh, *Proc. Natl. Acad. Sci. U. S. A.*, 2012, **109**, 10364–10369.
- 102 M. J. Footer, J. W. Kerssemakers, J. A. Theriot and M. Dogterom, *Proc. Natl. Acad. Sci. U. S. A.*, 2007, **104**, 2181–2186.
- 103 Q. Wen and P. A. Janmey, *Exp. Cell Res.*, 2013, **319**, 2481–2489.
- 104 H. Kang, Q. Wen, P. A. Janmey, J. X. Tang, E. Conti and F. C. MacKintosh, *J. Phys. Chem. B*, 2009, **113**, 3799–3805.
- 105 N. S. Gov, *New J. Phys.*, 2007, **9**, 429.
- 106 N. Gov and S. Safran, *Biophys. J.*, 2005, **88**, 1859–1874.
- 107 N. S. Gov, *Phys. Rev. E: Stat., Nonlinear, Soft Matter Phys.*, 2007, **75**, 011921.
- 108 B. Fabry, G. N. Maksym, J. P. Butler, M. Glogauer, D. Navajas, N. A. Taback, E. J. Millet and J. J. Fredberg, *Phys. Rev. E: Stat., Nonlinear, Soft Matter Phys.*, 2003, **68**, 041914.
- 109 K. M. Van Citters, B. D. Hoffman, G. Massiera and J. C. Crocker, *Biophys. J.*, 2006, **91**, 3946–3956.
- 110 S. Hiratsuka, Y. Mizutani, M. Tsuchiya, K. Kawahara, H. Tokumoto and T. Okajima, *Ultramicroscopy*, 2009, **109**, 937–941.
- 111 E. Moeendarbary, L. Valon, M. Fritzsche, A. R. Harris, D. A. Moulding, A. J. Thrasher, E. Stride, L. Mahadevan and G. T. Charras, *Nat. Mater.*, 2013, **12**, 253–261.
- 112 S. Kumar, I. Z. Maxwell, A. Heisterkamp, T. R. Polte, T. P. Lele, M. Salanga, E. Mazur and D. E. Ingber, *Biophys. J.*, 2006, **90**, 3762–3773.
- 113 S. Munavar, Y.-l. Wang and M. Dembo, *Biophys. J.*, 2001, **80**, 1744–1757.
- 114 D. Dikovsky, H. Bianco-Peled and D. Seliktar, *Biomaterials*, 2006, **27**, 1496–1506.

- 115 C. Franck, S. A. Maskarinec, D. A. Tirrell and G. Ravichandran, *PLoS One*, 2011, **6**, e17833.
- 116 X. Trepaut, L. Deng, S. S. An, D. Navajas, D. J. Tschumperlin, W. T. Gerthoffer, J. P. Butler and J. J. Fredberg, *Nature*, 2007, **447**, 592–595.
- 117 O. Loh, A. Vaziri and H. Espinosa, *Exp. Mech.*, 2009, **49**, 105–124.
- 118 G. M. Whitesides, *Nature*, 2006, **442**, 368–373.
- 119 D. Riveline, E. Zamir, N. Q. Balaban, U. S. Schwarz, T. Ishizaki, S. Narumiya, Z. Kam, B. Geiger and A. D. Bershadsky, *J. Cell Biol.*, 2001, **153**, 1175–1186.
- 120 R. Paul, P. Heil, J. P. Spatz and U. S. Schwarz, *Biophys. J.*, 2008, **94**, 1470–1482.
- 121 P. A. Janmey and C. A. McCulloch, *Annu. Rev. Biomed. Eng.*, 2007, **9**, 1–34.
- 122 P. Fernández, P. A. Pullarkat and A. Ott, *Biophys. J.*, 2006, **90**, 3796–3805.
- 123 P. Kollmannsberger and B. Fabry, *Annu. Rev. Mater. Res.*, 2011, **41**, 75–97.
- 124 B. D. Hoffman and J. C. Crocker, *Annu. Rev. Biomed. Eng.*, 2009, **11**, 259–288.
- 125 B. D. Hoffman, G. Massiera, K. M. Van Citters and J. C. Crocker, *Proc. Natl. Acad. Sci. U. S. A.*, 2006, **103**, 10259–10264.
- 126 S. Yamada, D. Wirtz and S. C. Kuo, *Biophys. J.*, 2000, **78**, 1736–1747.
- 127 L. Deng, X. Trepaut, J. P. Butler, E. Millet, K. G. Morgan, D. A. Weitz and J. J. Fredberg, *Nat. Mater.*, 2006, **5**, 636–640.
- 128 F. Wottawah, S. Schinkinger, B. Lincoln, S. Ebert, K. Müller, F. Sauer, K. Travis and J. Guck, *Acta Biomater.*, 2005, **1**, 263–271.
- 129 F. Wottawah, S. Schinkinger, B. Lincoln, R. Ananthakrishnan, M. Romeyke, J. Guck and J. Kärs, *Phys. Rev. Lett.*, 2005, **94**, 098103.
- 130 J. M. Maloney, D. Nikova, F. Lautenschläger, E. Clarke, R. Langer, J. Guck and K. J. Van Vliet, *Biophys. J.*, 2010, **99**, 2479–2487.
- 131 N. Desprat, A. Richert, J. Simeon and A. Asnacios, *Biophys. J.*, 2005, **88**, 2224–2233.
- 132 D. Stamenović, N. Rosenblatt, M. Montoya-Zavala, B. D. Matthews, S. Hu, B. Suki, N. Wang and D. E. Ingber, *Biophys. J.*, 2007, **93**, L39–L41.
- 133 E. Darling, S. Zauscher and F. Guilak, *Osteoarthritis and Cartilage*, 2006, **14**, 571–579.
- 134 S. Hu, J. Chen, J. P. Butler and N. Wang, *Biochem. Biophys. Res. Commun.*, 2005, **329**, 423–428.
- 135 S. Hu, J. Chen, B. Fabry, Y. Numaguchi, A. Gouldstone, D. E. Ingber, J. J. Fredberg, J. P. Butler and N. Wang, *Am. J. Physiol.: Cell Physiol.*, 2003, **285**, C1082–C1090.
- 136 D. Stamenović, B. Suki, B. Fabry, N. Wang, J. J. Fredberg and J. E. Buy, *J. Appl. Physiol.*, 2004, **96**, 1600–1605.
- 137 M. Escudé, M. K. Rigozzi and E. M. Terentjev, *Biophys. J.*, 2014, **106**, 124–133.
- 138 D. E. Ingber, *J. Cell Sci.*, 2003, **116**, 1157–1173.
- 139 D. E. Ingber, *J. Cell Sci.*, 2003, **116**, 1397–1408.
- 140 N. Wang, K. Naruse, D. Stamenović, J. J. Fredberg, S. M. Mijailovich, I. M. Tolić-Nurrelykke, T. Polte, R. Mannix and D. E. Ingber, *Proc. Natl. Acad. Sci. U. S. A.*, 2001, **98**, 7765–7770.
- 141 P. Cañadas, S. Wendling-Mansuy and D. Isabey, *J. Biomech. Eng.*, 2006, **128**, 487–495.
- 142 R. Blumenfeld, *Biophys. J.*, 2006, **91**, 1970–1983.
- 143 R. E. Laudadio, E. J. Millet, B. Fabry, S. S. An, J. P. Butler and J. J. Fredberg, *Am. J. Physiol.: Cell Physiol.*, 2005, **289**, C1388–C1395.
- 144 C. Y. Park, D. Tambe, A. M. Alencar, X. Trepaut, E. H. Zhou, E. Millet, J. P. Butler and J. J. Fredberg, *Am. J. Physiol.: Cell Physiol.*, 2010, **298**, C1245–C1252.
- 145 F. Ferri, M. Greco, G. Arcovito, M. De Spirito and M. Rocco, *Phys. Rev. E: Stat., Nonlinear, Soft Matter Phys.*, 2002, **66**, 011913.
- 146 C. Storm, J. J. Pastore, F. C. MacKintosh, T. C. Lubensky and P. A. Janmey, *Nature*, 2005, **435**, 191–194.
- 147 S. Münster, L. M. Jawerth, B. A. Leslie, J. I. Weitz, B. Fabry and D. A. Weitz, *Proc. Natl. Acad. Sci. U. S. A.*, 2013, **110**, 12197–12202.
- 148 M. K. Gordon and R. A. Hahn, *Cell Tissue Res.*, 2010, **339**, 247–257.
- 149 K. Gelse, E. Pöschl and T. Aigner, *Adv. Drug Delivery Rev.*, 2003, **55**, 1531–1546.
- 150 F. Grinnell and W. M. Petroll, *Annu. Rev. Cell Dev. Biol.*, 2010, **26**, 335–361.
- 151 F. H. M. Nestler, S. Hvidt, J. D. Ferry and A. Veis, *Biopolymers*, 1983, **22**, 1747–1758.
- 152 H. Utiyama, K. Sakato, K. Ikebara, T. Setsujiye and M. Kurata, *Biopolymers*, 1973, **12**, 53–64.
- 153 H. Hofmann, T. Voss, K. Kühn and J. Engel, *J. Mol. Biol.*, 1984, **172**, 325–343.
- 154 Y.-L. Sun, Z.-P. Luo, A. Fertala and K.-N. An, *Biochem. Biophys. Res. Commun.*, 2002, **295**, 382–386.
- 155 H. H. Lovelady, S. Shashidhara and W. G. Matthews, *Biopolymers*, 2013, **101**, 329–335.
- 156 M. J. Buehler, *J. Mech. Behav. Biomed. Mater.*, 2008, **1**, 59–67.
- 157 L. Yang, K. O. Van der Werf, C. F. Fitié, M. L. Bennink, P. J. Dijkstra and J. Feijen, *Biophys. J.*, 2008, **94**, 2204–2211.
- 158 R. C. Arevalo, J. S. Urbach and D. L. Blair, *Biophys. J.*, 2010, **99**, L65–L67.
- 159 A. M. Stein, D. A. Vader, D. A. Weitz and L. M. Sander, *Complexity*, 2011, **16**, 22–28.
- 160 A. M. Stein, D. A. Vader, L. M. Jawerth, D. A. Weitz and L. M. Sander, *J. Microsc.*, 2008, **232**, 463–475.
- 161 P. P. Provenzano and R. Vanderby Jr, *Matrix Biol.*, 2006, **25**, 71–84.
- 162 J. A. van der Rijt, K. O. van der Werf, M. L. Bennink, P. J. Dijkstra and J. Feijen, *Macromol. Biosci.*, 2006, **6**, 697–702.
- 163 A. Gautieri, S. Vesentini, A. Redaelli and M. J. Buehler, *Nano Lett.*, 2011, **11**, 757–766.
- 164 A. Masic, L. Bertinetto, R. Schuetz, L. Galvis, N. Timofeeva, J. W. Dunlop, J. Seto, M. A. Hartmann and P. Fratzl, *Biomacromolecules*, 2011, **12**, 3989–3996.
- 165 P. Fratzl and R. Weinkamer, *Prog. Mater. Sci.*, 2007, **52**, 1263–1334.

- 166 P. Fratzl, K. Misof, I. Zizak, G. Rapp, H. Amenitsch and S. Bernstorff, *J. Struct. Biol.*, 1998, **122**, 119–122.
- 167 S. Rigozzi, A. Stemmer, R. Müller and J. Snedeker, *J. Struct. Biol.*, 2011, **176**, 9–15.
- 168 C. M. Kiely, M. J. Sherratt and C. A. Shuttleworth, *J. Cell Sci.*, 2002, **115**, 2817–2828.
- 169 S. Shapiro, S. Endicott, M. Province, J. Pierce and E. Campbell, *J. Clin. Invest.*, 1991, **87**, 1828.
- 170 C. Baldock, A. F. Oberhauser, L. Ma, D. Lammie, V. Siegler, S. M. Mithieux, Y. Tu, J. Y. H. Chow, F. Suleman and M. Malfois, *Proc. Natl. Acad. Sci. U. S. A.*, 2011, **108**, 4322–4327.
- 171 G. C. Yeo, C. Baldock, A. Tuukkanen, M. Roessle, L. B. Dyksterhuis, S. G. Wise, J. Matthews, S. M. Mithieux and A. S. Weiss, *Proc. Natl. Acad. Sci. U. S. A.*, 2012, **109**, 2878–2883.
- 172 S. M. Mithieux, S. G. Wise and A. S. Weiss, *Adv. Drug Delivery Rev.*, 2012, **65**, 421–428.
- 173 J. Holst, S. Watson, M. S. Lord, S. S. Eamegdool, D. V. Bax, L. B. Nivison-Smith, A. Kondyurin, L. Ma, A. F. Oberhauser and A. S. Weiss, *Nat. Biotechnol.*, 2010, **28**, 1123–1128.
- 174 B. Aaron and J. Gosline, *Biopolymers*, 1981, **20**, 1247–1260.
- 175 T. Rozario and D. W. DeSimone, *Dev. Biol.*, 2010, **341**, 126–140.
- 176 S. P. Lake, K. S. Miller, D. M. Elliott and L. J. Soslowsky, *J. Orthop. Res.*, 2009, **27**, 1596–1602.
- 177 K. S. Miller, B. K. Connizzo, E. Feeney, J. J. Tucker and L. J. Soslowsky, *J. Biomed. Eng.*, 2012, **134**, 041004.
- 178 K. S. Miller, B. K. Connizzo, E. Feeney and L. J. Soslowsky, *J. Biomech.*, 2012, **45**, 2061–2065.
- 179 F. Cacho, P. J. Elbischger, J. F. Rodrguez, M. Doblar and G. A. Holzapfel, *Int. J. Nonlinear Mech.*, 2007, **42**, 391–402.
- 180 M. B. Lilledahl, B. Skallerud and C. Davies, *Proc. SPIE*, 2009, **7183**, 718325.
- 181 J. Gosline, M. Lillie, E. Carrington, P. Guerette, C. Ortlepp and K. Savage, *Philos. Trans. R. Soc., B*, 2002, **357**, 121–132.
- 182 K. D. Smith, A. Vaughan-Thomas, D. G. Spiller, J. F. Innes, P. D. Clegg and E. J. Comerford, *J. Anat.*, 2011, **218**, 600–607.
- 183 H. Oxlund, J. Manschot and A. Viidik, *J. Biomech.*, 1988, **21**, 213–218.
- 184 B. C. Starcher, *Chest*, 2000, **117**, 229S–234S.
- 185 J. Schrauwen, A. Vilanova, R. Rezakhanlha, N. Stergiopoulos, F. Van De Vosse and P. Bovendeerd, *J. Struct. Biol.*, 2012, **180**, 335–342.
- 186 J. Löbler, R. Timpl and R. Jaenisch, *Cell*, 1984, **38**, 597–607.
- 187 T. Watanabe, Y. Imamura, D. Suzuki, Y. Hosaka, H. Ueda, K. Hiramatsu and K. Takehana, *J. Anat.*, 2012, **220**, 156–163.
- 188 M. Franchi, A. Trirè, M. Quaranta, E. Orsini and V. Ottani, *Sci. World J.*, 2007, **7**, 404–420.
- 189 M. Kjær, *Physiol. Rev.*, 2004, **84**, 649–698.
- 190 P. Panwar, X. Du, V. Sharma, G. Lamour, M. Castro, H. Li and D. Brömmel, *J. Biol. Chem.*, 2013, **288**, 5940–5950.
- 191 S. Vesentini, A. Redaelli and F. M. Montevercchi, *J. Biomech.*, 2005, **38**, 433–443.
- 192 G. Fessel and J. G. Snedeker, *J. Theor. Biol.*, 2011, **268**, 77–83.
- 193 H. Ahmadzadeh, B. K. Connizzo, B. R. Freedman, L. J. Soslowsky and V. B. Shenoy, *J. Biomech.*, 2013, **46**, 2497–2503.
- 194 P. Kannus, *Scand. J. Med. Sci. Sports*, 2000, **10**, 312–320.
- 195 I. Gusachenko, V. Tran, Y. G. Houssen, J.-M. Allain and M.-C. Schanne-Klein, *Biophys. J.*, 2012, **102**, 2220–2229.
- 196 K. A. Hansen, J. A. Weiss and J. K. Barton, *J. Biomech. Eng.*, 2002, **124**, 72–77.
- 197 R. B. Svensson, P. Hansen, T. Hassenkam, B. T. Haraldsson, P. Aagaard, V. Kovanen, M. Krogsgaard, M. Kjaer and S. P. Magnusson, *J. Appl. Physiol.*, 2012, **112**, 419–426.
- 198 T. Nagel and D. J. Kelly, *Biomech. Model. Mechanobiol.*, 2012, **11**, 325–339.
- 199 P. L. Chandran and V. H. Barocas, *J. Biomech. Eng.*, 2006, **128**, 259.
- 200 J. Adkins and R. Rivlin, *Philos. Trans. R. Soc., A*, 1955, **248**, 201–223.
- 201 Y. Lanir, *J. Biomech.*, 1983, **16**, 1–12.
- 202 R. Rezakhanlha, A. Agianniotis, J. Schrauwen, A. Griffa, D. Sage, C. Bouten, F. Vosse, M. Unser and N. Stergiopoulos, *Biomech. Model. Mechanobiol.*, 2012, **11**, 461–473.
- 203 G. A. Holzapfel and R. W. Ogden, *Proc. R. Soc. A*, 2010, **466**, 1551–1597.